



TECH BRIEFS

NATIONAL AERONAUTICS AND SPACE ADMINISTRATION

-  **Technology Focus**
-  **Electronics/Computers**
-  **Software**
-  **Materials**
-  **Mechanics/Machinery**
-  **Manufacturing**
-  **Bio-Medical**
-  **Physical Sciences**
-  **Information Sciences**
-  **Books and Reports**
-  **Green Design**

INTRODUCTION

Tech Briefs are short announcements of innovations originating from research and development activities of the National Aeronautics and Space Administration. They emphasize information considered likely to be transferable across industrial, regional, or disciplinary lines and are issued to encourage commercial application.

Availability of NASA Tech Briefs and TSPs

Requests for individual Tech Briefs or for Technical Support Packages (TSPs) announced herein should be addressed to

National Technology Transfer Center

Telephone No. (800) 678-6882 or via World Wide Web at www.nttc.edu

Please reference the control numbers appearing at the end of each Tech Brief. Information on NASA's Innovative Partnerships Program (IPP), its documents, and services is also available at the same facility or on the World Wide Web at <http://www.nasa.gov/offices/ipp/network/index.html>

Innovative Partnerships Offices are located at NASA field centers to provide technology-transfer access to industrial users. Inquiries can be made by contacting NASA field centers listed below.

Ames Research Center

Mary Walsh
(650) 604-1405
mary.w.walsh@nasa.gov

Dryden Flight Research Center

Yvonne D. Gibbs
(661) 276-3720
yvonne.d.gibbs@nasa.gov

Glenn Research Center

Joe Shaw, Acting Chief
(216) 977-7135
robert.j.shaw@nasa.gov

Goddard Space Flight Center

Nona Cheeks
(301) 286-5810
nona.k.cheeks@nasa.gov

Jet Propulsion Laboratory

Indrani Graczyk
(818) 354-2241
indrani.graczyk@jpl.nasa.gov

Johnson Space Center

information
(281) 483-3809
jsc.techtran@mail.nasa.gov

Kennedy Space Center

David R. Makufka
(321) 867-6227
david.r.makufka@nasa.gov

Langley Research Center

Elizabeth B. Plentovich
(757) 864-2857
elizabeth.b.plentovich@nasa.gov

Marshall Space Flight Center

Jim Dowdy
(256) 544-7604
jim.dowdy@msfc.nasa.gov

Stennis Space Center

Ramona Travis
(228) 688-3832
ramona.e.travis@nasa.gov

Carl Ray, Program Executive

Small Business Innovation
Research (SBIR) & Small
Business Technology
Transfer (STTR) Programs
(202) 358-4652
carl.g.ray@nasa.gov

Doug Comstock, Partnerships

Innovation and Commercial
Space Program Office (formerly IPP)
(202) 358-2221
doug.comstock@nasa.gov



TECH BRIEFS

NATIONAL AERONAUTICS AND SPACE ADMINISTRATION



5 Technology Focus: Sensors

- 5 Amperometric Solid Electrolyte Oxygen Microsensors With Easy Batch Fabrication
- 5 Two-Axis Direct Fluid Shear Stress Sensor for Aerodynamic Applications
- 6 Target Assembly to Check Boresight Alignment of Active Sensors
- 7 Virtual Sensor Test Instrumentation



9 Electronics/Computers

- 9 Evaluation of the Reflection Coefficient of Microstrip Elements for Reflectarray Antennas
- 9 Miniaturized Ka-Band Dual-Channel Radar
- 10 Continuous-Integration Laser Energy Lidar Monitor
- 10 Miniaturized Airborne Imaging Central Server System
- 11 Radiation-Tolerant, SpaceWire-Compatible Switching Fabric



13 Semiconductors & ICs

- 13 Small Microprocessor for ASIC or FPGA Implementation
- 13 Source-Coupled, N-Channel, JFET-Based Digital Logic Gate Structure Using Resistive Level Shifters
- 13 High-Voltage-Input Level Translator Using Standard CMOS
- 14 Monitoring Digital Closed-Loop Feedback Systems



17 Software

- 17 MASCOT — MATLAB Stability and Control Toolbox
- 17 MIRO Continuum Calibration for Asteroid Mode
- 17 GOATS Image Projection Component
- 18 Coded Modulation in C and MATLAB



19 Manufacturing & Prototyping

- 19 Low-Dead-Volume Inlet for Vacuum Chamber
- 19 Thermal Control Method for High-Current Wire Bundles by Injecting a Thermally Conductive Filler
- 19 Method for Selective Cleaning of Mold Release From Composite Honeycomb Surfaces
- 20 Infrared-Bolometer Arrays With Reflective Backshorts



21 Materials

- 21 Commercialization of LARC™-SI Polyimide Technology
- 21 Novel Low-Density Ablators Containing Hyperbranched Poly(azomethine)s

- 22 Carbon Nanotubes on Titanium Substrates for Stray Light Suppression



23 Mechanics/Machinery

- 23 Monolithic, High-Speed Fiber-Optic Switching Array for Lidar



25 Green Design

- 25 Grid-Tied Photovoltaic Power System
- 25 Spectroelectrochemical Instrument Measures TOC



27 Bio-Medical

- 27 A Miniaturized Video System for Monitoring Drosophila Behavior
- 27 Hydrofocusing Bioreactor Produces Anti-Cancer Alkaloids



29 Physical Sciences

- 29 Creep Measurement Video Extensometer
- 29 Radius of Curvature Measurement of Large Optics Using Interferometry and Laser Tracker
- 30 n-B-pi-p Superlattice Infrared Detector



31 Information Sciences

- 31 Safe Onboard Guidance and Control Under Probabilistic Uncertainty
- 31 General Tool for Evaluating High-Contrast Coronagraphic Telescope Performance Error Budgets
- 31 Hidden Statistics of Schrödinger Equation
- 32 Optimal Padding for the Two-Dimensional Fast Fourier Transform
- 32 Spatial Query for Planetary Data
- 33 Higher Order Mode Coupling in Feed Waveguide of a Planar Slot Array Antenna
- 33 Evolutionary Computational Methods for Identifying Emergent Behavior in Autonomous Systems
- 34 Sampling Theorem in Terms of the Bandwidth and Sampling Interval



35 Books & Reports

- 35 Meteoroid/Orbital Debris Shield Engineering Development Practice and Procedure
- 35 Self-Balancing, Optical-Center-Pivot, Fast-Steering Mirror
- 35 Wireless Orbiter Hang-Angle Inclinometer System
- 35 Internal Electrostatic Discharge Monitor — IESDM

This document was prepared under the sponsorship of the National Aeronautics and Space Administration. Neither the United States Government nor any person acting on behalf of the United States Government assumes any liability resulting from the use of the information contained in this document, or warrants that such use will be free from privately owned rights.



Amperometric Solid Electrolyte Oxygen Microsensors With Easy Batch Fabrication

These microsensors are applicable to fire detection, environmental monitoring, fuel leak detection, and engine emission monitoring.

John H. Glenn Research Center, Cleveland, Ohio

There is a great need for oxygen microsensors for aerospace and commercial applications. Current bulk or thick-film solid electrolyte oxygen sensors have the disadvantages of being large in size, high in power consumption, difficult to batch-fabricate, and high in cost.

An amperometric solid electrolyte oxygen (O₂) microsensor using a novel and robust structure has been developed with a detection range of 0.025 to 21 percent of O₂ concentration. The microsensor has a simple structure with a sensing area of 1.10×0.99 mm², and is operated by applying voltage across the electrodes and measuring the resulting current flow at a temperature of 600 °C.

Semiconductor microfabrication techniques are used in the sensor fabrication. The fabrication of oxygen microsensors includes two steps: deposition of platinum interdigitated finger electrodes, and deposition of yttria stabilized zirconia (YSZ) on the finger electrodes. The platinum interdigitated finger electrodes were deposited as follows: Alumina substrates (250 μm in thickness) were patterned with photoresist and an interdigitated finger elec-

trode photomask. A layer of 50 Å of titanium and a layer of 2,500 Å of platinum were deposited on the substrate by sputter deposition. After photoresist liftoff, the solid electrolyte YSZ was deposited on top of the electrode area by sputtering using a shadow mask. The sensor testing is conducted by applying a voltage to the electrodes and measuring the resulting current.

The novel and important aspect of the development is that, instead of applying an extra structure on top of the sensor surface, which involves very complicated fabrication processes, the YSZ itself is used as both a diffusion barrier and sensing layer. Therefore, a thicker YSZ layer than that used in other structures is deposited. The extra YSZ thickness prevents the sensor from being saturated by high concentrations of oxygen gases. This novel approach enabled a simpler sensor structure, easier batch fabrication process, higher sensor yield, and lower cost.

Another important aspect is that while the extra thickness of the YSZ is meant to be a diffusion barrier, it also contributes to the current output of the

sensor. By adjusting the YSZ thickness, different detection ranges can be achieved. At 7,500 Å, the sensor has a viable detection range of 0.025 to 16 percent, with a linear response to the logarithm of oxygen concentrations. By increasing the thickness of solid electrolyte YSZ to 2.6 μm, the O₂ detection range has been expanded to higher concentrations; an overall range of 0.025 to 21 percent is achieved.

The microsensor has a wide detection range and high current output considering its size. It can be integrated into a sensor array with other sensors and electronics, power, and telemetry on a postage-stamp-sized package as part of a smart sensor system.

This work was done by Gary W. Hunter and Jennifer C. Xu of Glenn Research Center and Chung-Chium Liu of Case Western Reserve University. Further information is contained in a TSP (see page 1).

Inquiries concerning rights for the commercial use of this invention should be addressed to NASA Glenn Research Center, Innovative Partnerships Office, Attn: Steven Fedor, Mail Stop 4-8, 21000 Brookpark Road, Cleveland, Ohio 44135. Refer to LEW-18592-1.

Two-Axis Direct Fluid Shear Stress Sensor for Aerodynamic Applications

This microsensor, fabricated using MEMS technology to enable low-cost production, makes truly nonintrusive biaxial shear stress measurements.

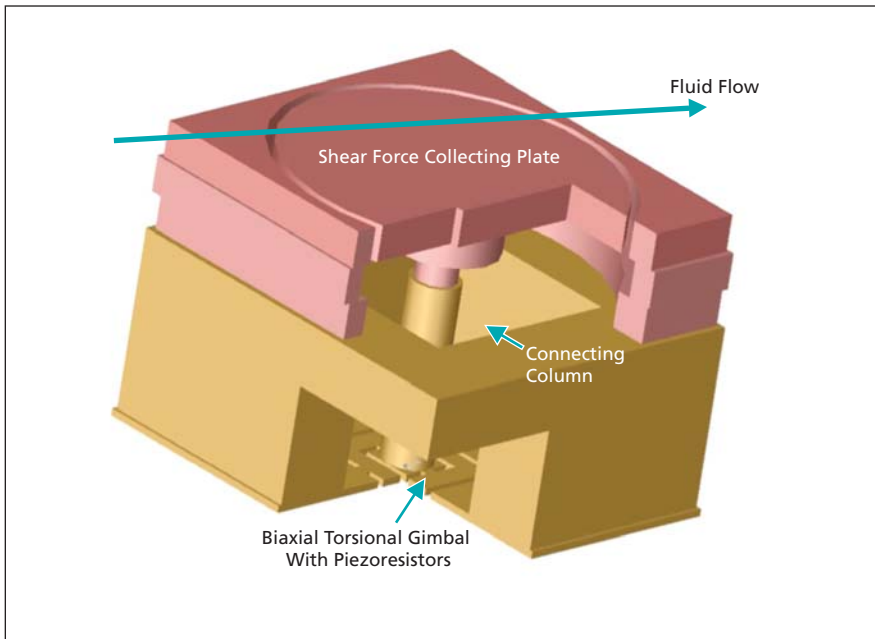
Goddard Space Flight Center, Greenbelt, Maryland

This miniature or micro-sized semiconductor sensor design provides direct, nonintrusive measurement of skin friction or wall shear stress in fluid flow situations in a two-axis configuration. The sensor is fabricated by microelectromechanical system (MEMS) technology, enabling small size and multiple, low-cost reproductions. The sensors may be fabri-

cated by bonding a sensing element wafer to a fluid-coupling element wafer. Using this layered machine structure provides a truly three-dimensional device.

The sensor design (see figure) includes a shear-force collecting plate (fluid-coupling element) with dimensions tailored to application-determined resolutions (spatial, temporal,

and force). The plate is located coplanar to both the sensor body and flow boundary. This plate is coupled to a biaxial gimbal structure provided with piezoresistors on its torsional hinges, and, located parallel to but some distance from the force collection plate, with a connecting column. This design thus allows a nonintrusive method to



This Sensor is designed for nonintrusive measurement of the shear force on aerodynamic bodies.

qualitatively measure the shear force vector on aerodynamic bodies.

The sensors themselves are typically made in single crystal silicon with the piezoresistor elements formed by doping the silicon (by ion implantation or other means) to a suitable type and level

of conductivity that provides the desired sensitivity depending on the crystal orientation. Metallic electrical leads on the back face of the device are provided to route excitation currents and output signal voltages from these sensors to the external world.

Subjecting the plate of the device to a shear force, by mounting it on an aerodynamic surface exposed to flow, will result in a moment acting on the hinges of the biaxial gimbal structure that is proportional to the shear stress on the plate, the arm, and torsional hinge dimensions. This moment creates a mechanical torsional shear stress within the hinges and, thereby, an output signal proportional to the shear stress on the plate from the piezoresistive sensor. The shear stress at the fluid-sensor interfaces is thus initially converted to a mechanical shear stress in the hinge that is sensed with a piezoresistive sensor. The two orthogonally located hinges and sensors enable measuring the shear stress existing on the plate in both directions. This configuration of the sensor device enables a large moment and stress level to be generated at the hinge from relatively small shear stress acting on a small plate, thereby enabling high spatial and stress resolution capability.

This work was done by Sateesh S. Bajjkar of Goddard Space Flight Center and Michael A. Scott and Edward E. Adcock of Langley Research Center. Further information is contained in a TSP (see page 1). GSC-15431-1

Target Assembly to Check Boresight Alignment of Active Sensors

This assembly can simultaneously measure the co-boresite alignment of multiple transmitter laser beams and receiver channels.

Goddard Space Flight Center, Greenbelt, Maryland

A compact and portable target assembly (Fig. 1) has been developed to measure the boresite alignment of LRO's Lunar Orbiter Laser Altimeter (LOLA) instrument at the spacecraft level. The concept for this target assembly has evolved over many years with earlier versions used to test the Mars Observer Laser Altimeter (MOLA), the Geoscience Laser Altimeter System (GLAS), and the Mercury Laser Altimeter (MLA) space-based instruments. These earlier laser altimeters were single ranging channel instruments, but as demonstrated with the five-channel LOLA instrument, the target assembly can simultaneously measure the co-boresite alignment of multiple transmitter laser beams and receiver channels (Fig. 2).

The target assembly flips the transmitter laser beam into the optical re-

ceiver aperture and measures their co-alignment error by scanning the laser far-field image across the receiver field-of-view (FOV) in two orthogonal axes. Plotting the receiver response as a function of the transmitter beam de-

viation angle yields the effective laser altimeter transceiver alignment. The target assembly components include a Laser Beam Dump (LBD) to attenuate the input laser energy by an order of magnitude, a lateral transfer retro-re-

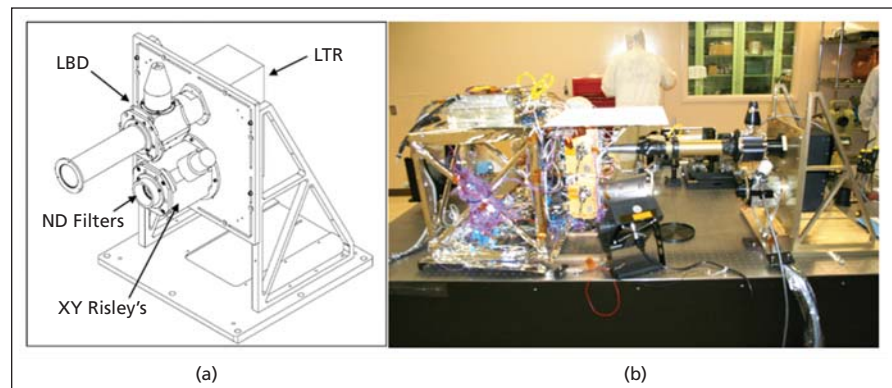


Fig. 1. Target Assembly: (a) LOLA target assembly components, (b) LOLA instrument test with target assembly.

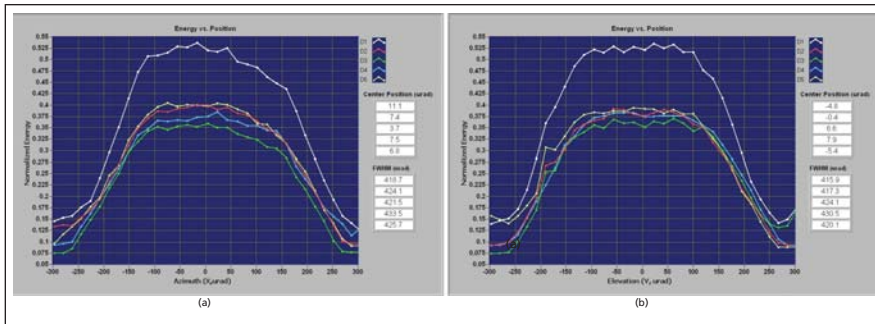


Fig. 2. LOLA Laser 1 S/C Level Bore-site Alignment Test Results: (a) X-Axis, (b) Y-Axis.

flector (LTR) to flip the transmitter laser beam by exactly 180° into the receiver telescope, a set of motorized and computer-controlled Risley prisms to scan the transmitter laser beam across the receiver FOV in a controlled and measurable fashion, and a set of parallel plate neutral density (ND) fil-

ters to attenuate the output laser beam by several orders of magnitude to a receiver-safe level.

The target assembly is compact, modular, accurate, and easy to use. The target assembly itself is alignment insensitive, so no special care needs to be taken in placing the target assembly

in front of the instrument under test other than making sure that the transmitter laser beam is not vignetted at the target assembly entrance aperture. In addition, sealing the transmitter path to the target assembly input aperture is usually required to prevent stray light from saturating or damaging the sensitive receiver detector(s) of the instrument under test. The target assembly components can be easily changed to customize the target assembly for any required active sensor co-alignment measurement task.

This work was performed by Luis Ramos-Izquierdo, V. Stanley Scott, Haris Riris, and John Cavanaugh of Goddard Space Flight Center, and Peter Liiva and Michael Rodriguez of Sigma Space Corporation. Further information is contained in a TSP (see page 1). GSC-15789-1

Virtual Sensor Test Instrumentation

This technology has application in wireless RFID systems.

Stennis Space Center, Mississippi

Virtual Sensor Test Instrumentation is based on the concept of smart sensor technology for testing with intelligence needed to perform self-diagnosis of health, and to participate in a hierarchy of health determination at sensor, process, and system levels. A virtual sensor test instrumentation consists of five elements: (1) a common sensor interface, (2) microprocessor, (3) wireless interface, (4) signal conditioning and ADC/DAC (analog-to-digital conversion/digital-to-analog conversion), and (5) onboard EEPROM (electrically erasable programmable read-only memory) for metadata storage and executable software to create powerful, scalable, reconfigurable, and reliable embedded and distributed test instruments. In order to maximize the efficient data conversion through the smart sensor node, plug-and-play functionality is required to interface with traditional sensors to enhance their identity and capabilities for data processing and communications.

Virtual sensor test instrumentation can be accessible wirelessly via a Network Capable Application Processor (NCAP)

or a Smart Transducer Interlace Module (STIM) that may be managed under real-time rule engines for mission-critical applications.

The transducer senses the physical quantity being measured and converts it into an electrical signal. The signal is fed to an A/D converter, and is ready for use by the processor to execute functional transformation based on the sensor characteristics stored in a Transducer Electronic Data Sheet (TEDS). Virtual sensor test instrumentation is built upon an open-system architecture with standardized protocol modules/stacks to interface with industry standards and commonly used software. One major benefit for deploying the virtual sensor test instrumentation is the ability, through a plug-and-play common interface, to convert raw sensor data in either analog or digital form, to an IEEE 1451 standard-based smart sensor, which has instructions to program sensors for a wide variety of functions. The sensor data is processed in a distributed fashion across the network, providing a large pool of resources in real time to meet stringent latency requirements. Advantages of de-

ploying the virtual sensor test instrumentation include:

- Simplification of troubleshooting through HTML/XML-based Health Monitoring that allows the user to verify all sensors via a graphic user interface.
- Cost reduction for set-up and tear-down through sensor auto detection.
- Elimination of recalibration when replacing sensors. The data acquisition system can recalibrate itself through TEDS.
- Elimination of large lengths of analog wiring through a radio frequency module.
- Reduction of installation, maintenance, and upgrade costs of measurement and control systems through Web-based TEDS server.
- Increased opportunity to add intelligence to sensors through embedded EEPROM.

This work was done by Ray Wang for Stennis Space Center.

*For more information, contact:
Mobitrum Corporation
Phone No.: (301) 585-4040
Refer to SSC-00336.*



Evaluation of the Reflection Coefficient of Microstrip Elements for Reflectarray Antennas

NASA's Jet Propulsion Laboratory, Pasadena, California

Basis functions were studied and identified that provide efficient and accurate solutions for the induced patch currents and the reflection phase in microstrip reflectarrays. The integral equation of an infinite array of microstrip elements in the form of patches or crossed dipoles excited by a uniform plane wave is solved by the method-of-moments. Efficient choices of entire domain basis functions that yield accurate results have been described.

The results showed that an optimum choice would be a sinusoidal basis func-

tion with a built-in edge condition along the current flow direction, and uniform current across the current flow direction for a rectangular or square patch. For a dipole, the optimum choice is a sinusoidal basis function without the edge condition along the dipole, and uniform with the edge condition across. The code employing these basis functions was substantially faster than the commercial code HFSS, and it was significantly more accurate than previously developed method-of-moments code.

It was determined that the optimum choice is one basis function for each of the two induced currents in a square or rectangular patch, and one basis function for each dipole. For very thin substrates, there was a need to have 32 basis functions to produce accurate solutions.

This work was done by Sembiam Rengarajan of Caltech for NASA's Jet Propulsion Laboratory. For more information, contact iaofice@jpl.nasa.gov. NPO-47449

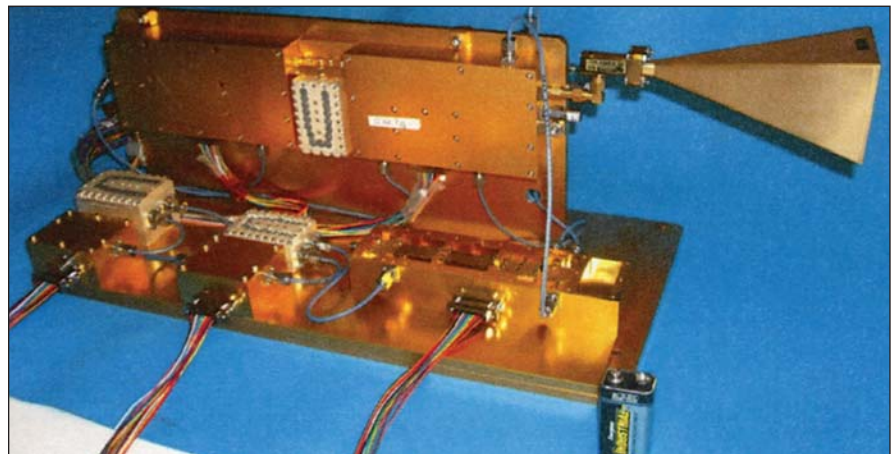
Miniaturized Ka-Band Dual-Channel Radar

This smaller, higher-bandwidth system can be used for interferometry, ocean surface height monitoring, and various military applications.

NASA's Jet Propulsion Laboratory, Pasadena, California

Smaller (volume, mass, power) electronics for a Ka-band (36 GHz) radar interferometer were required. To reduce size and achieve better control over RF-phase versus temperature, fully hybrid electronics were developed for the RF portion of the radar's two-channel receiver and single-channel transmitter. In this context, fully hybrid means that every active RF device was an open die, and all passives were directly attached to the subcarrier. Attachments were made using wire and ribbon bonding. In this way, every component, even small passives, was selected for the fabrication of the two radar receivers, and the devices were mounted relative to each other in order to make complementary components isothermal and to isolate other components from potential temperature gradients. This is critical for developing receivers that can track each other's phase over temperature, which is a key mission driver for obtaining ocean surface height.

Fully hybrid, Ka-band (36 GHz) radar transmitter and dual-channel receiver were developed for spaceborne radar interferometry. The fully hybrid fabrication enables control over every aspect



The fully integrated Ka-Band Dual-Channel Radar with horn antenna. The transmitter electronics are shown along the baseplate, while the dual receivers are mounted on the vertical plate. The last stage of the transmitter is left open to show the subcarriers.

of the component selection, placement, and connection. Since the two receiver channels must track each other to better than 100 millidegrees of RF phase over several minutes, the hardware in the two receivers must be "identical," routed the same (same line lengths), and as isothermal as possible. This level of design freedom is not possible with packaged components, which include

many internal passive, unknown internal connection lengths/types, and often a single orientation of inputs and outputs.

The last item is key to fabricating a dual-channel receiver, where one wants components from the two channels to be isothermal, and therefore mounted back-to-back, while also having the routing as similar as possible. This

drives the design to be mirrored, where the two channels are fabricated back-to-back, achieving direct mechanical interface to improve the isothermal performance, which drives RF phase balance. This back-to-back design forces components to have a “left” and “right” handed version, which is not typically possible for packaged components, but with full design control of hybrid design, this is achievable. The radar was designed to have a series of

separate subcarriers, which could be hermetically sealed individually, which is much easier than sealing the entire unit. Also, in the event of late component failure, rather than losing or reworking the entire unit, the subcarrier can easily be replaced by another qualified subcarrier.

This new instrument is a smaller, higher-bandwidth dual-channel interferometer with 500-MHz bandwidth at Ka-band (35.5 to 36 GHz), as compared to

the prior instrument WSOA (Wide Swath Ocean Altimeter), which was Ku-band (13.275 GHz) with 80-MHz bandwidth. The new instrument has six-fold improvement in resolution capability, and better control of factors that contribute to RF phase stability.

This work was done by James P. Hoffman, Alina Moussessian, Masud Jenabi, and Brian Custodero of Caltech for NASA’s Jet Propulsion Laboratory. Further information is contained in a TSP (see page 1). NPO-47346

Continuous-Integration Laser Energy Lidar Monitor

The integrator can be used in developing pulsed lasers for space-based lidar and ground-based laser applications.

Goddard Space Flight Center, Greenbelt, Maryland

This circuit design implements an integrator intended to allow digitization of the energy output of a pulsed laser, or the energy of a received pulse of laser light. It integrates the output of a detector upon which the laser light is incident. The integration is performed constantly, either by means of an active integrator, or by passive components. If an active integrator is used, closed-loop dc biasing is added with a time constant much longer than the laser pulse width. The output of the integrator goes to a track-and-hold amplifier (THA), using a zero-potential switch topology. The track/hold control is derived from timing information obtained either by a threshold comparator on the detector, or a peak detector. Laser pulses of varying widths can be accommodated by adjusting the characteristics of the timing control circuitry. The output of the THA

is available for digitization at a later time. Bandwidth limiting can be used in the signal path as necessary, depending on the noise characteristics of the signal.

Prior integration techniques utilize threshold comparators to “start” and “stop” the integration. Some implementations require reset circuitry, which can create offset at the output. Starting and stopping the integration usually involves clipping off the beginning and/or end of the signal; this introduces greater errors as the signal amplitude decreases. Also, as the signal speed increases, the comparator speed must increase, and thus its power consumption rises. As the signal (pulse) gets narrower, the comparator delay time may cut off significant portions of the signal unless electronic delay is introduced. This adds complexity, mass, and timing uncertainty.

The advantage of this integration technique is that it does not depend on

exact threshold adjustment to start or stop the integrator, nor does it require the use of switches to discharge the integration capacitor. Further, there is no pedestal introduced in the integrator.

This circuit is intended to implement an integrator that does not require time gating, delay, or reset circuitry, in order to avoid the limitations that these elements impose. The integrator is part of a pulsed laser energy monitor. This implementation of a continuous integrator is designed to be used in a laser transmit energy monitor.

The final design had the ability to integrate pulses down to 50 mV at 4.5 ns, and 250 mV at 3 ns, with 0.8-percent electrical accuracy.

This work was done by Jeremy Karsh of Goddard Space Flight Center. Further information is contained in a TSP (see page 1). GSC-15843-1

Miniaturized Airborne Imaging Central Server System

This imaging server can be used for natural disaster response and for locating new sources of spring water.

Goddard Space Flight Center, Greenbelt, Maryland

In recent years, some remote-sensing applications require advanced airborne multi-sensor systems to provide high performance reflective and emissive spectral imaging measurement rapidly over large areas. The key or unique problem of characteristics is associated with a black box back-end system that operates a suite of cutting-edge imaging sensors to collect simultaneously the high

throughput reflective and emissive spectral imaging data with precision georeference. This back-end system needs to be portable, easy-to-use, and reliable with advanced onboard processing.

The innovation of the black box back-end is a miniaturized airborne imaging central server system (MAICSS). MAICSS integrates a complex embedded system of systems with dedicated power and sig-

nal electronic circuits inside to serve a suite of configurable cutting-edge electro-optical (EO), long-wave infrared (LWIR), and medium-wave infrared (MWIR) cameras, a hyperspectral imaging scanner, and a GPS and inertial measurement unit (IMU) for atmospheric and surface remote sensing. Its compatible sensor packages include NASA’s 1,024×1,024 pixel LWIR quantum well in-

frared photodetector (QWIP) imager; a 60.5 megapixel BuckEye EO camera; and a fast (e.g. 200+ scanlines/s) and wide swath-width (e.g., 1,920+ pixels) CCD/InGaAs imager-based visible/near infrared reflectance (VNIR) and short-wave infrared (SWIR) imaging spectrometer. MAICSS records continuous precision georeferenced and time-tagged multisensor throughputs to mass storage devices at a high aggregate rate, typically 60 MB/s for its LWIR/EO payload.

MAICSS is a complete stand-alone imaging server instrument with an easy-to-use software package for either autonomous data collection or interactive airborne operation. Advanced multisensor data acquisition and onboard processing software features have been implemented for MAICSS. With the

onboard processing for real time image development, correction, histogram-equalization, compression, georeference, and data organization, fast aerial imaging applications, including the real time LWIR image mosaic for Google Earth, have been realized for NASA's LWIR QWIP instrument.

MAICSS is a significant improvement and miniaturization of current multisensor technologies. Structurally, it has a complete modular and solid-state design. Without rotating hard drives and other moving parts, it is operational at high altitudes and survivable in high-vibration environments. It is assembled from a suite of miniaturized, precision-machined, standardized, and stackable interchangeable embedded instrument modules. These stackable modules can

be bolted together with the interconnection wires inside for the maximal simplicity and portability. Multiple modules are electronically interconnected as stacked. Alternatively, these dedicated modules can be flexibly distributed to fit the space constraints of a flying vehicle. As a flexibly configurable system, MAICSS can be tailored to interface a variety of multisensor packages. For example, with a 1,024×1,024 pixel LWIR and a 8,984×6,732 pixel EO payload, the complete MAICSS volume is approximately 7×9×11 in. (≈18×23×28 cm), with a weight of 25 lb (≈11.4 kg).

This work was done by Xiuhong Sun of Flight Landata for Goddard Space Flight Center. Further information is contained in a TSP (see page 1). GSC-15817-1

Radiation-Tolerant, SpaceWire-Compatible Switching Fabric

Potential applications include next-generation computer interconnects, production of motion pictures, intra-hospital networks, and inventory management.

Goddard Space Flight Center, Greenbelt, Maryland

Current and future near-Earth and deep space exploration programs and space defense programs require the development of robust intra-spacecraft serial data transfer electronics that must be reconfigurable, fault-tolerant, and have the ability to operate effectively for long periods of time in harsh environmental conditions. Existing data transfer systems based on state-of-the-art serial data transfer protocols or passive backplanes are slow, power-hungry, and poorly reconfigurable. They provide limited expandability and poor tolerance to radiation effects and total ionizing dose (TID) in particular, which presents harmful threats to modern submicron electronics.

This novel approach is based on a standard library of differential cells tolerant to TID, and patented, multi-level serial interface architecture that ensures the reliable operation of serial interconnects without application of a data-strobe or other encoding techniques. This proprietary, high-speed differential interface presents a low-power solution fully compatible with the SpaceWire (SW) protocol. It replaces a dual data-strobe link with two identical independent data channels, thus improving the system's tolerance to harsh environments through additional double redundancy. Each chan-

nel incorporates an automatic line integrity control circuitry that delivers error signals in case of broken or shorted lines.

The complete 4×4 SW switching fabric chip (with dimensions 6,618×5,658 mm²), incorporating the switching fabric core synthesized in a standard radiation-tolerant by-process 180-nm CMOS (complementary metal oxide semiconductor) library and four proprietary interfaces, has been fully designed in a BiCMOS technology from Jazz Semiconductor and prepared for fabrication. All critical blocks of the switching fabric have been verified through fabrication of several test chips and demonstrated the radiation tolerance up to TID = 1 MRad. All main blocks of the fabric have been developed as IP (intellectual property) macro-blocks ready to be integrated into other systems in order to minimize the design time, efforts, and risk.

The complete architecture of a 4×4 switching fabric with selectable SW or ML interfaces has been developed based on the Core code supplied by NASA. The architecture of a custom SW/ML routing port has been developed and evaluated. Based on the detailed investigations, the SiGe120 BiCMOS technology has been selected for the implementation of the proposed

SF. A complete library of CML (Chemical Markup Language) cells with full anti-TID and anti-SEE protection by architecture (SPBA) has been developed and simulated. The designed SPBA library has been fully characterized to make it suitable for automatic synthesis procedures. Special techniques required for the adaptation of the new differential library to existing single-ended synthesis software tools have been developed and verified.

A complex test chip based on the SPBA library has been fabricated and tested. The measurement results gathered in accordance with the developed test plan demonstrated the efficiency of the selected approach for the implementation of high-duty logic functions and SerDes systems in particular. The provided SF Core has been fully synthesized and simulated in the SPBA library. In an attempt to minimize the power consumption, the SF Core was re-synthesized in the foundry-provided standard CMOS library. This approach, in combination with a CML-based implementation of routing ports, proved to be optimal.

This work was done by Vladimir Katzman of ADSANTEC for Goddard Space Flight Center. Further information is contained in a TSP (see page 1). GSC-15818-1



Small Microprocessor for ASIC or FPGA Implementation

Goddard Space Flight Center, Greenbelt, Maryland

A small microprocessor, suitable for use in applications in which high reliability is required, was designed to be implemented in either an application-specific integrated circuit (ASIC) or a field-programmable gate array (FPGA). The design is based on commercial microprocessor architecture, making it possible to use available software development tools and thereby to implement the microprocessor at relatively low cost. The design features enhancements, including trapping during execution of il-

legal instructions. The internal structure of the design yields relatively high performance, with a significant decrease, relative to other microprocessors that perform the same functions, in the number of microcycles needed to execute macroinstructions.

The problem meant to be solved in designing this microprocessor was to provide a modest level of computational capability in a general-purpose processor while adding as little as possible to the power demand, size, and weight of a

system into which the microprocessor would be incorporated. As designed, this microprocessor consumes very little power and occupies only a small portion of a typical modern ASIC or FPGA. The microprocessor operates at a rate of about 4 million instructions per second with clock frequency of 20 MHz.

This work was done by Igor Kleyner, Richard Katz, and Hugh Blair-Smith of Goddard Space Flight Center. Further information is contained in a TSP (see page 1). GSC-15493-1

Source-Coupled, N-Channel, JFET-Based Digital Logic Gate Structure Using Resistive Level Shifters

John H. Glenn Research Center, Cleveland, Ohio

A circuit topography is used to create usable, digital logic gates using N (negatively doped) channel junction field effect transistors (JFETs), load resistors, level shifting resistors, and supply rails whose values are based on the DC parametric distributions of these JFETs. This method has direct application to the current state-of-the-art in high-temperature (300 to 500 °C and higher) silicon carbide (SiC) device production, and defines an adaptation to the logic gate described in U.S. Patent 7,688,117 in that, by removing the level shifter from the output of the gate structure described in the patent (and applying it to the input of the same gate), a source-

coupled gate topography is created. This structure allows for the construction AND/OR (sum of products) arrays that use far fewer transistors and resistors than the same array as constructed from the gates described in the aforementioned patent. This plays a central role when large multiplexer constructs are necessary; for example, as in the construction of memory.

This innovation moves the resistive level shifter from the output of the basic gate structure to the front as if the input is now configured as what would be the output of the preceding gate, wherein the output is the two level shifting resistors. The output of this innovation can

now be realized as the lone follower transistor with its source node as the gate output. Additionally, one may leave intact the resistive level shifter on the new gate topography. A source-coupled to direct-coupled logic translator will be the result.

This work was done by Michael J. Krasowski of Glenn Research Center. Further information is contained in a TSP (see page 1).

Inquiries concerning rights for the commercial use of this invention should be addressed to NASA Glenn Research Center, Innovative Partnerships Office, Attn: Steven Fedor, Mail Stop 4-8, 21000 Brookpark Road, Cleveland, Ohio 44135. Refer to LEW-18636-1.

High-Voltage-Input Level Translator Using Standard CMOS

High-voltage input circuitry would be combined with standard low-voltage CMOS circuitry.

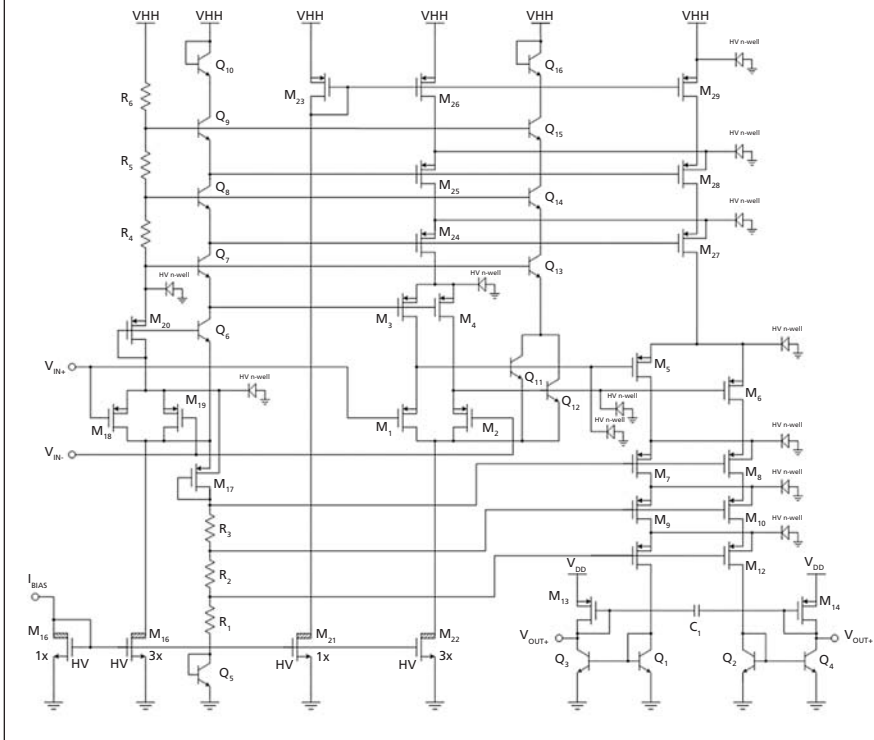
NASA's Jet Propulsion Laboratory, Pasadena, California

A proposed integrated circuit would translate (1) a pair of input signals having a low differential potential and a possibly high common-mode potential into (2) a pair of output signals having the same low differential potential and a low common-mode potential. As used

here, "low" and "high" refer to potentials that are, respectively, below or above the nominal supply potential (3.3 V) at which standard complementary metal oxide/semiconductor (CMOS) integrated circuits are designed to operate. The input common-mode potential

could lie between 0 and 10 V; the output common-mode potential would be 2 V. This translation would make it possible to process the pair of signals by use of standard 3.3-V CMOS analog and/or mixed-signal (analog and digital) circuitry on the same integrated-circuit

Input Common-Mode Range	0.3 to 10V
-3 dB Bandwidth	150 kHz
Common-Mode Rejection Ratio	>80 dB
Power Supply Rejection Ratio	>50 dB
Noise Characteristics	
MOS Flicker Noise@ 1Hz	≈ 90 nV/√Hz
Flicker Noise Corner	≈ 800 Hz
Broadband Noise	≈ 55 nV/√Hz



Several Performance Parameters of the proposed level translator were extracted from results of computational simulations. The proposed circuit schematic is shown.

chip. A schematic of the circuit is shown in the figure.

Standard 3.3-V CMOS circuitry cannot withstand input potentials greater than about 4 V. However, there are many applications that involve low-differential-potential, high-common-mode-potential input signal pairs and in which standard 3.3-V CMOS circuitry, which is relatively inexpensive, would be the most appropriate

circuitry for performing other functions on the integrated-circuit chip that handles the high-potential input signals. Thus, there is a need to combine high-voltage input circuitry with standard low-voltage CMOS circuitry on the same integrated-circuit chip. The proposed circuit would satisfy this need.

In the proposed circuit, the input signals would be coupled into both a level-

shifting pair and a common-mode-sensing pair of CMOS transistors. The output of the level-shifting pair would be fed as input to a differential pair of transistors. The resulting differential current output would pass through six standoff transistors to be mirrored into an output branch by four heterojunction bipolar transistors. The mirrored differential current would be converted back to potential by a pair of diode-connected transistors, which, by virtue of being identical to the input transistors, would reproduce the input differential potential at the output.

The common-mode-sensing pair would be used to set the control potential for a biasing circuit that would provide the proper terminal potentials for protecting all devices against excessive excursions of potential for a common-mode potential range of 0 to 12 V. The biasing circuit would include high-voltage-drain transistors capable of withstanding the full high input potentials on their drains; the incorporation of these transistors would enable simplification of part of the bias circuit and of the circuitry associated with the input transistor pairs. High-voltage n-wells would enable floating of substrates of p-channel metal oxide/semiconductor field-effect transistors to potentials as high as tens of volts, whereas devices containing standard n-wells break down at potentials between 6 and 7 V, even though maximum gate-to-source and drain-to-source potentials remain at 3.3 V.

The expected performance of the circuit has been studied in computational simulations. The table presents values of some performance parameters determined from the results of the simulations.

This work was done by Jeremy A. Yager, Mohammad M. Mojarradi, and Tuan A. Vo of Caltech and Benjamin J. Blalock from University of Tenn., Knoxville for NASA's Jet Propulsion Laboratory. Further information is contained in a TSP (see page 1). NPO-45762

Monitoring Digital Closed-Loop Feedback Systems

Designed-in test circuitry enables determination of performance margins and performance trends.

Goddard Space Flight Center, Greenbelt, Maryland

A technique of monitoring digital closed-loop feedback systems has been conceived. The basic idea is to obtain information on the performances of closed-loop feedback circuits in such systems to aid in the determination of the functionality and integrity of the circuits and of performance margins.

The need for this technique arises as follows: Some modern digital systems include feedback circuits that enable other circuits to perform with precision and are tolerant of changes in environment and the device's parameters. For example, in a precision timing circuit, it is desirable to make the circuit insensitive to variability as a re-

sult of the manufacture of circuit components and to the effects of temperature, voltage, radiation, and aging. However, such a design can also result in masking the indications of damaged and/or deteriorating components.

The present technique incorporates test circuitry and associated engineering-

telemetry circuitry into an embedded system to monitor the closed-loop feedback circuits, using “spare gates” that are often available in field programmable gate arrays (FPGAs). This technique enables a test engineer to determine the amount of performance margin in the system, detect “out of family” circuit performance, and determine one or more trend(s) in the performance of the system.

In one system to which the technique has been applied, an ultra-stable oscillator is used as a reference for internal adjustment of 12 time-to-digital converters (TDCs). The feedback circuit produces a pulse-width-modulated signal that is fed

as a control input into an amplifier, which controls the circuit’s operating voltage. If the circuit’s gates are determined to be operating too slowly or rapidly when their timing is compared with that of the reference signal, then the pulse width increases or decreases, respectively, thereby commanding the amplifier to increase or reduce, respectively, its output level, and “adjust” the speed of the circuits. The nominal frequency of the TDC’s pulse width modulated outputs is approximately 40 kHz.

In this system, the technique is implemented by means of a monitoring circuit that includes a 20-MHz sampling circuit

and a 24-bit accumulator with a gate time of 10 ms. The monitoring circuit measures the duty cycle of each of the 12 TDCs at a repetition rate of 28 Hz. The accumulator content is reset to all zeroes at the beginning of each measurement period and is then incremented or decremented based of the value of the state of the pulse width modulated signal. Positive or negative values in the accumulator correspond to duty cycles greater or less, respectively, than 50 percent.

This work was done by Richard Katz and Igor Kleyner of Goddard Space Flight Center. Further information is contained in a TSP (see page 1). GSC-15489-1



🌀 MASCOT — MATLAB Stability and Control Toolbox

MASCOT software was created to provide the conceptual aircraft designer accurate predictions of air vehicle stability and control characteristics. The code takes as input mass property data in the form of an inertia tensor, aerodynamic loading data, and propulsion (i.e. thrust) loading data. Using fundamental non-linear equations of motion, MASCOT then calculates vehicle trim and static stability data for any desired flight condition. Common predefined flight conditions are included. The predefined flight conditions include six horizontal and six landing rotation conditions with varying options for engine out, crosswind and sideslip, plus three takeoff rotation conditions. Results are displayed through a unique graphical interface developed to provide stability and control information to the conceptual design engineers using a qualitative scale indicating whether the vehicle has acceptable, marginal, or unacceptable static stability characteristics.

This software allows the user to prescribe the vehicle's CG location, mass, and inertia tensor so that any loading configuration between empty weight and maximum take-off weight can be analyzed. The required geometric and aerodynamic data as well as mass and inertia properties may be entered directly, passed through data files, or come from external programs such as Vehicle Sketch Pad (VSP). The current version of MASCOT has been tested with VSP used to compute the required data, which is then passed directly into the program. In VSP, the vehicle geometry is created and manipulated. The aerodynamic coefficients, stability and control derivatives, are calculated using VorLax, which is now available directly within VSP. MASCOT has been written exclusively using the technical computing language MATLAB®.

This innovation is able to bridge the gap between low-fidelity conceptual design and higher-fidelity stability and control analysis. This new tool enables the conceptual design engineer to include detailed static stability and trim constraints in the conceptual design loop. The unique graphical interface devel-

oped for this tool presents the stability data in a format that is understandable by the conceptual designer, yet also provides the detailed quantitative results if desired.

This work was done by Sean Kenny of Langley Research Center and Luis Crespo of the National Institute of Aerospace. Further information is contained in a TSP (see page 1), LAR-16581-1

🌀 MIRO Continuum Calibration for Asteroid Mode

MIRO (Microwave Instrument for the Rosetta Orbiter) is a lightweight, uncooled, dual-frequency heterodyne radiometer. The MIRO encountered asteroid Steins in 2008, and during the flyby, MIRO used the Asteroid Mode to measure the emission spectrum of Steins. The Asteroid Mode is one of the seven modes of the MIRO operation, and is designed to increase the length of time that a spectral line is in the MIRO pass-band during a flyby of an object. This software is used to calibrate the continuum measurement of Steins' emission power during the asteroid flyby.

The MIRO raw measurement data need to be calibrated in order to obtain physically meaningful data. This software calibrates the MIRO raw measurements in digital units to the brightness temperature in Kelvin. The software uses two calibration sequences that are included in the Asteroid Mode. One sequence is at the beginning of the mode, and the other at the end. The first six frames contain the measurement of a cold calibration target, while the last six frames measure a warm calibration target. The targets have known temperatures and are used to provide reference power and gain, which can be used to convert MIRO measurements into brightness temperature.

The software was developed to calibrate MIRO continuum measurements from Asteroid Mode. The software determines the relationship between the raw digital unit measured by MIRO and the equivalent brightness temperature by analyzing data from calibration frames. The found relationship is applied to non-calibration frames, which are the measurements of an object of interest such as asteroids and other

planetary objects that MIRO encounters during its operation.

This software characterizes the gain fluctuations statistically and determines which method to estimate gain between calibration frames. For example, if the fluctuation is lower than a statistically significant level, the averaging method is used to estimate the gain between the calibration frames. If the fluctuation is found to be statistically significant, a linear interpolation of gain and reference power is used to estimate the gain between the calibration frames.

This work was done by Seungwon Lee of Caltech for NASA's Jet Propulsion Laboratory. Further information is contained in a TSP (see page 1).

The software used in this innovation is available for commercial licensing. Please contact Daniel Broderick of the California Institute of Technology at danielb@caltech.edu. Refer to NPO-47075.

🌀 GOATS Image Projection Component

When doing mission analysis and design of an imaging system in orbit around the Earth, answering the fundamental question of imaging performance requires an understanding of the image products that will be produced by the imaging system. At the highest level, this understanding can be gained by a first-principles analysis of the geometric image projections involved in image capture from space. Going back to first principles allows for requirements to be quickly analyzed and the fundamental specifications of the imaging systems to be tweaked and traded quickly to aid in rapid mission design and analysis. The problem then becomes encapsulating these first-principle algorithms in a set of easy-to-use and modular functions to be used in coordination with other mission design tools.

GOATS software represents a series of MATLAB functions to provide for geometric image projections. Unique features of the software include function modularity, a standard MATLAB interface, easy-to-understand first-principles-based analysis, and the ability to perform geometric image projections of framing type imaging systems. The software modules are created for maximum analysis utility, and can all be used inde-

pendently for many varied analysis tasks, or used in conjunction with other orbit analysis tools.

By basing the tools purely on first principles and utilizing a high degree of generalization, the same set of tools can be applied to imaging systems not in orbit (i.e., helicopters, high-altitude planes, etc.). The image projection tools begin with a simple description of the imaging system to be analyzed. This description is based on the highest level of imaging parameters (system F-number, pixel pitch, aperture size, etc.), which are among the first parameters settled upon when contemplating a new system. The tools are structured this way to allow for early analysis of the highest level requirements and the performance of rather detailed trade studies to best settle upon these high-level requirements early on.

Using these high-level parameters and the imaging geometry of the proposed system, one can geometrically project the imaging system onto the ground and determine many of the features of the collected imagery. These features include ground sample distances, actual image size and geolocation, image stretching and warping, etc. With these features calculated, there is a direct link between imaging system hardware parameters and performance requirements. Additionally, the same tools can be used to do some level of image processing. Existing image data

sets can be processed and re-projected to simulate what they would look like had they been taken with an imaging system with different parameters. The functions provide a robust toolset to quickly answer several types of imaging questions that typically arise when considering missions around framing imaging systems.

This work was done by Benjamin M. Haber and Joseph J. Green of Caltech for NASA's Jet Propulsion Laboratory. For more information, contact iaoffice@jpl.nasa.gov.

This software is available for commercial licensing. Please contact Daniel Broderick of the California Institute of Technology at danielb@caltech.edu. Refer to NPO-47281.

Coded Modulation in C and MATLAB

This software, written separately in C and MATLAB as stand-alone packages with equivalent functionality, implements encoders and decoders for a set of nine error-correcting codes and modulators and demodulators for five modulation types. The software can be used as a single program to simulate the performance of such coded modulation.

The error-correcting codes implemented are the nine accumulate repeat-4 jagged accumulate (AR4JA) low-density parity-check (LDPC) codes, which have been approved for international standardization by the Consultative Committee for Space Data Systems, and

which are scheduled to fly on a series of NASA missions in the Constellation Program. The software implements the encoder and decoder functions, and contains compressed versions of generator and parity-check matrices used in these operations.

The software supports the modulations of binary phase-shift keying (BPSK), quadrature PSK (QPSK), 8-PSK, 16-ary amplitude PSK (16-APSK), and 32-APSK. For each modulation type, the software modulator supports various bit-to-modulation-symbol mappings, including the natural order, the Gray code, the anti-Gray code, and the ordering specified by the Digital Video Broadcast Satellite Second Generation standard for 16-APSK and 32-APSK. The software supports hard and soft demodulation, and when soft, it supports both an exact log likelihood computation and an approximate log likelihood computation based on nearest neighbors.

The software supports all nine AR4JA LDPC codes of the CCSDS standard and all five modulations of the DVB-S2 standard, in any combination.

This work was done by Jon Hamkins and Kenneth S. Andrews of Caltech for NASA's Jet Propulsion Laboratory. For more information, contact iaoffice@jpl.nasa.gov.

This software is available for commercial licensing. Please contact Daniel Broderick of the California Institute of Technology at danielb@caltech.edu. Refer to NPO-47171.



Low-Dead-Volume Inlet for Vacuum Chamber

John F. Kennedy Space Center, Florida

Gas introduction from near-ambient pressures to high vacuum traditionally is accomplished either by multi-stage differential pumping that allows for very rapid response, or by a capillary method that allows for a simple, single-stage introduction, but which often has a delayed response. Another means to introduce the gas sample is to use the multi-stage design with only a single

stage. This is accomplished by using a very small conductance limit. The problem with this method is that a small conductance limit will amplify issues associated with dead-volume.

As a result, a high-vacuum gas inlet was developed with low dead-volume, allowing the use of a very low conductance limit interface. Gas flows through the ConFlat flange at a relatively high flow

rate at orders of magnitude greater than through the conductance limit. The small flow goes through a conductance limit that is a double-sided ConFlat.

This work was done by Guy Naylor and C. Arkin of ASRC Aerospace Corporation for Kennedy Space Center. For further information, contact the Kennedy Innovative Partnerships Program Office at (321) 861-7158. KSC-13317

Thermal Control Method for High-Current Wire Bundles by Injecting a Thermally Conductive Filler

Goddard Space Flight Center, Greenbelt, Maryland

A procedure was developed to inject thermal filler material (a paste-like substance) inside the power wire bundle coming from solar arrays. This substance fills in voids between wires, which enhances the heat path and reduces wire temperature. This leads to a reduced amount of heat generated. This technique is especially helpful for current and future generation high-power spacecraft (1 kW or more), because the heat generated by the power wires is significant enough to cause unacceptable overheating to critical components that are in close contact with the bundle.

Powered test results in thermal vacuum showed a significant decrease in

temperature with filler of ≈ 50 °C. Without filler, the bulk wire temperature was around 100 °C, whereas with filler, it was around 50 °C. The heat generated by the bundle was reduced by ≈ 15 percent. The procedure generated the development of an injection manifold for simultaneous injection around the perimeter of the bundle, which is unique. This manifold ensures a consistent and thorough fill of gaps between wires.

The unique or novel features are twofold. This is the first instance where thermal filler material was used to fill in voids in between wires to enhance thermal path, and reduce wire temperatures and heat generated. The injection man-

ifold designed for the procedure is also unique. A thermal test was performed in order to evaluate the advantages of the use of this procedure. In the test with 2.5 A running through the wires, an approximately 50 °C temperature reduction was measured after the filler injection procedure. Heat conduction path improved by up to a factor of 11, and waste heat generated was reduced by 15 percent.

This work was done by Juan Rodriguez-Ruiz, Russell Rowles, and Greg Greer of Goddard Space Flight Center. Further information is contained in a TSP (see page 1). GSC-15987-1

Method for Selective Cleaning of Mold Release From Composite Honeycomb Surfaces

A simple, EPA-friendly approach solves a long-standing problem in heat-formed composite manufacturing.

Goddard Space Flight Center, Greenbelt, Maryland

Honeycomb structures are commonly employed as load- and force-bearing structures as they are structurally strong and lightweight. These structures include many aircraft and spacecraft surfaces, including aircraft wings and fuselages, spacecraft pressure vessels, and heat-shield materials.

Many other processes in other areas of transportation and defense, as well as the pharmaceutical and construction industries, employ pressure vessels with similar heat-formed composite structures.

Manufacturing processes for heat-molded composite honeycomb structures

commence with the placement of pre-impregnated composite layups over metal mandrels. To prevent permanent bonding between the composite layup and the metal mandrels, an agent, known as a mold release agent, is used. Mold release agents allow the molded composite mate-

rial to be removed from mandrels after a heat-forming process. Without a specific removal process, mold release agents may continue to adhere to the surface of the composite material, thereby affecting the bonding of other materials that may come into contact with the composite surface in later stages of processing.

Mold release agents have a unique chemistry that, upon heating, requires a unique chemical method for removal. Prior art includes immersion solvent cleaning (trichloroethylene, hexane, limonene), vapor degreasing, and plasma cleaning. Many of the solvent and vapor degreasing techniques, such as Freon and trichloroethylene, can no longer be used per EPA standards.

Plasma cleaning has limited use in structures that have a deep channel or high aspect ratio, as the plasma penetrates diffusively and thus, may result in incomplete cleaning for the full depth of the structure.

A constituent common to commercially available household cleaning agents is employed for the removal of mold release agents common to the manufacturing of heat-formed composite materials. The reliability of the solvent has been proven by the longevity and reliability of commercial household cleaners. At the time of this reporting, no one has attempted using constituent for this purpose. The material to be cleaned is immersed in the solution, vertically re-

moved so that the solution is allowed to drain along cell walls and into a solvent bath, and then placed on a compressed airflow table for drying. Non-destructive evaluation techniques [see "Non-Destructive Evaluation of Materials via Ultraviolet Spectroscopy" (GSC-15338), *NASA Tech Briefs*, Vol. 32, No. 6 (June 2008) p. 81] are employed to detect mold release residue and evaluate the degree of cleanliness. The cleaning process is repeated until non-destructive evaluation shows minimal detection limits for mold release residue.

This work was done by Diane Pugel of Goddard Space Flight Center. Further information is contained in a TSP (see page 1). GSC-15902-1

Infrared-Bolometer Arrays With Reflective Backshorts

Operational wavelengths can be tailored by adjusting a few process steps.

Goddard Space Flight Center, Greenbelt, Maryland

Integrated circuits that incorporate square arrays of superconducting-transition-edge bolometers with optically reflective backshorts are being developed for use in image sensors in the spectral range from far infrared to millimeter wavelengths. To maximize the optical efficiency (and, thus, sensitivity) of such a sensor at a specific wavelength, resonant optical structures are created by placing the backshorts at a quarter wavelength behind the bolometer plane. The bolometer and backshort arrays are fabricated separately, then integrated to form a single unit denoted a backshort-under-grid (BUG) bolometer array. In a subsequent fabrication step, the BUG bolometer array is connected, by use of single-sided indium bump bonding, to a readout device that comprises mostly a superconducting quantum interference device (SQUID) multiplexer circuit. The resulting sensor unit comprising the BUG bolometer array and the readout device is operated at a temperature below 1 K.

The concept of increasing optical efficiency by use of backshorts at a quarter wavelength behind the bolometers is not new. Instead, the novelty of the present development lies mainly in several features of the design of the BUG bolometer array and the fabrication sequence used to implement the design. Prior to joining with the backshort array, the bolometer array comprises, more specifically, a square grid of free-standing molybdenum/gold superconducting-transition-edge bolometer elements on a 1.4- μm -thick top layer of silicon that is part of a silicon support frame made from a silicon-on-insulator wafer. The backshort array is fabricated separately as a frame structure that includes support beams and contains a corresponding grid of optically reflective patches on a single-crystal silicon substrate.

The process used to fabricate the bolometer array includes standard patterning and etching steps that result in the formation of deep notches in the sili-

con support frame. These notches are designed to interlock with the support beams on the backshort-array structure to provide structural support and precise relative positioning. The backshort-array structure is inserted in the silicon support frame behind the bolometer array, and the notches in the frame serve to receive the support beams of the backshort-array structure and thus determine the distance between the backshort and bolometer planes. The depth of the notches and, thus, the distance between the backshort and bolometer planes, can be tailored to a value between 25 to 300 μm adjusting only a few process steps. The backshort array is designed so as not to interfere with the placement of indium bumps for subsequent indium bump-bonding to the multiplexing readout circuitry.

This work was done by Timothy M. Miller, John Abrahams, and Christine A. Allen of Goddard Space Flight Center. Further information is contained in a TSP (see page 1). GSC-15104-1



Commercialization of LARC™-SI Polyimide Technology

The resulting material is now used in medical, aircraft, consumer products, and electronics applications.

Langley Research Center, Hampton, Virginia

LARC™-SI, Langley Research Center-Soluble Imide, was developed in 1992, with the first patent issuing in 1997, and then subsequent patents issued in 1998 and 2000. Currently, this polymer has been successfully licensed by NASA, and has generated revenues, at the time of this reporting, in excess of \$1.4 million. The success of this particular polymer has been due to many factors and many lessons learned to the point that the invention, while important, is the least significant part in the commercialization of this material.

Commercial LARC™-SI is a polyimide composed of two molar equivalents of dianhydrides: 4,4'-oxydiphthalic anhydride (ODPA), and 3,3',4,4'-biphenyltetracarboxylic dianhydride (BPDA) and 3,4'-oxydianiline (3,4'-ODA) as the diamine. The unique feature of this aromatic polyimide is that it remains soluble after solution imidization in high-boiling, polar aprotic solvents, even at solids contents of 50-percent by weight. However, once isolated and heated above its T_g of 240 °C, it becomes insoluble and exhibits high-temperature thermoplastic melt-flow behavior. With these unique structure property characteristics, it was thought this would be an advantage to have an aromatic poly-

imide that is both solution and melt processable in the imide form. This could potentially lead to lower cost production as it was not as equipment- or labor-intensive as other high-performance polyimide materials that either precipitate or are intractable.

This unique combination of properties allowed patents with broad claim coverage and potential commercialization. After the U.S. Patent applications were filed, a Small Business Innovation Research (SBIR) contract was awarded to Imtec, Inc. to develop and supply the polyimide to NASA and the general public. Some examples of demonstration parts made with LARC™-SI ranged from aircraft wire and multilayer printed-circuit boards, to gears, composite panels, supported adhesive tape, composite coatings, cookware, and polyimide foam. Even with its unique processing characteristics, the thermal and mechanical properties were not drastically different from other solution or melt-processable polyimides developed by NASA. LARC™-SI risked becoming another interesting, but costly, high-performance material.

A licensee was sought, and a specific application was developed, the THUNDER piezoelectric actuator. This actua-

tor used the polyimide as the adhesive to thermally bond metal shims to the piezoelectric ceramic. This gave the THUNDER actuator a mechanical pre-stress, resulting in enhanced solid-state motion. Because this actuator had separate fields of use, and all the test data was developed using LARC™-SI as one of the components, the commercial THUNDER actuator used LARC™-SI as the adhesive, and was thus partially responsible for keeping LARC™-SI in the public spotlight.

Both LARC™-SI and THUNDER were licensed to several companies, including a known company that was actively investing in marketing a material developed by NASA (Dominion Resources, Inc.). It was important to find a large company that had continuous sales of high-value-added products that could support the initial price and benefit from the use of an expensive new material to gain market share. It was a medical products industry company that licensed LARC™-SI for use as a new wire varnish for pacemaker leads, an application that was never envisioned.

This work was done by Robert G. Bryant for Langley Research Center. Further information is contained in a TSP (see page 1). LARC-15205-1

Novel Low-Density Ablators Containing Hyperbranched Poly(azomethine)s

John H. Glenn Research Center, Cleveland, Ohio

An ablative composite is low-density (0.25 to 0.40 g/cm³), easy to fabricate, and superior to the current state-of-the-art ablator (phenolic impregnated carbon ablator, PICA) in terms of decomposition temperature, char yield, and mechanical strength. Initial ablative testing with a CO₂ laser under high-heat-flux (1,100 W/cm²) conditions showed these new ablators are over twice as effective as PICA in terms of

weight loss, as well as transfer of heat through the specimen.

The carbon fiber/poly(azomethine) composites have the same density as PICA, but are 8 to 11 times stronger to irreversible breaking by tensile compression. In addition, polyazomethine char yields by thermogravimetric analysis are 70 to 80 percent at 1,000 °C. This char yield is 10 to 20 percent higher than phenolic resins, as well as one of the highest

char yields known for any polymer. A high char yield holds the composite together better toward shearing forces on reentry, as well as reradiates high heat fluxes. This innovative composite is stronger than PICA, so multiple pieces can be sealed together without fracture.

Researchers have also studied polyazomethines before as linear polymers. Due to poor solubility, these polymers precipitate from the polymerization sol-

vent as a low-molecular-weight (2 to 4 repeat units) powder. The only way found to date to keep linear polyazomethines in solution is by adding solubilizing side groups. However, these groups sacrifice certain polymer properties. These hy-

perbranched polyazomethines are high molecular weight and fully aromatic.

This work was done by Dean Tigelaar of Ohio Aerospace Institute for Glenn Research Center. Further information is contained in a TSP (see page 1).

Inquiries concerning rights for the commercial use of this invention should be addressed to NASA Glenn Research Center, Innovative Partnerships Office, Attn: Steven Fedor, Mail Stop 4-8, 21000 Brookpark Road, Cleveland, Ohio 44135. Refer to LEW-18642-1.

Carbon Nanotubes on Titanium Substrates for Stray Light Suppression

Goddard Space Flight Center, Greenbelt, Maryland

A method has been developed for growing carbon nanotubes on a titanium substrate, which makes the nanotubes ten times blacker than the current state-of-the-art paints in the visible to near infrared. This will allow for significant improvement of stray light performance in scientific instruments, or any other optical system.

Because baffles, stops, and tubes used in scientific observations often undergo loads such as vibration, it is

critical to develop this surface treatment on structural materials. This innovation optimizes the carbon nanotube growth for titanium, which is a strong, lightweight structural material suitable for spaceflight use. The steps required to grow the nanotubes require the preparation of the surface by lapping, and the deposition of an iron catalyst over an alumina stiction layer by e-beam evaporation.

In operation, the stray light controls are fabricated, and nanotubes (multi-walled 100 microns in length) are grown on the surface. They are then installed in the instruments or other optical devices.

This work was done by John Hagopian, Stephanie Getty, and Manuel Quijada of Goddard Space Flight Center. Further information is contained in a TSP (see page 1). GSC-16016-1



Monolithic, High-Speed Fiber-Optic Switching Array for Lidar

Electro-optic crystals allow for fast, multi-fiber switching without moving parts.

NASA's Goddard Space Flight Center, Greenbelt, Maryland

Current fiber switch technologies use mechanical means to redirect light beams, resulting in slow switch time, as well as poor reliability due to moving parts wearing out quickly at high speeds. A non-mechanical ability to switch laser output into one of multiple fibers within a fiber array can provide significant power, weight, and costs savings to an all-fiber system.

This invention uses an array of crystals that act as miniature prisms to redirect light as an electric voltage changes the prism's properties. At the heart of the electro-optic fiber-optic switch is an electro-optic crystal patterned with tiny prisms that can deflect the beam from

the input fiber into any one of the receiving fibers arranged in a linear array when a voltage is applied across the crystal. Prism boundaries are defined by a net dipole moment in the crystal lattice that has been poled opposite to the surrounding lattice fabricated using patterned, removable microelectrodes. When a voltage is applied across the crystal, the resulting electric field changes the index of refraction within the prism boundaries relative to the surrounding substrate, causing light to deflect slightly according to Snell's Law.

There are several materials that can host the necessary monolithic poled pat-

tern (including, but not limited to, SLT, KTP, LiNbO₃, and Mg:LiNbO₃). Because this is a solid-state system without moving parts, it is very fast, and does not wear down easily.

This invention is applicable to all fiber networks, as well as industries that use such networks. The unit comes in a compact package, can handle both low and high voltages, and has a high reliability (100,000 hours without maintenance).

This work was done by Will Suckow, Tony Roberts, Gregg Switzer, and Chelle Terwilliger of AdvR, Inc. for Goddard Space Flight Center. Further information is contained in a TSP (see page 1). GSC-15627-1



Grid-Tied Photovoltaic Power System

This method can be used for generating clean, sustainable electric power.

John H. Glenn Research Center, Cleveland, Ohio

A grid-tied photovoltaic (PV) power system is connected directly to the utility distribution grid. Facility power can be obtained from the utility system as normal. The PV system is synchronized with the utility system to provide power for the facility, and excess power is provided to the utility.

Operating costs of a PV power system are low compared to conventional power technologies. This method can displace the highest-cost electricity during times of peak demand in most climatic regions, and thus reduce grid loading. Net metering is often used, in which independent power producers such as PV power systems are connected to the utility grid via the customers' main service panels and meters. When the PV power system is generating more power than required at that location, the excess power is provided to the utility

grid. The customer pays the net of the power purchased when the on-site power demand is greater than the on-site power production, and the excess power is returned to the utility grid.

Power generated by the PV system reduces utility demand, and the surplus power aids the community. Modern PV panels are readily available, reliable, efficient, and economical, with a life expectancy of at least 25 years. Modern electronics have been the enabling technology behind grid-tied power systems, making them safe, reliable, efficient, and economical with a life expectancy equal to the modern PV panels.

The grid-tied PV power system was successfully designed and developed, and this served to validate the basic principles developed, and the theoretical work that was performed. Grid-tied PV power systems are reliable, mainte-

nance-free, long-life power systems, and are of significant value to NASA and the community. Of particular value are the analytical tools and capabilities that have been successfully developed. Performance predictions can be made confidently for grid-tied PV systems of various scales. The work was done under the NASA Hybrid Power Management (HPM) Program, which is the integration of diverse power devices in an optimal configuration for space and terrestrial applications.

This work was done by Dennis J. Eichenberg of Glenn Research Center. Further information is contained in a TSP (see page 1).

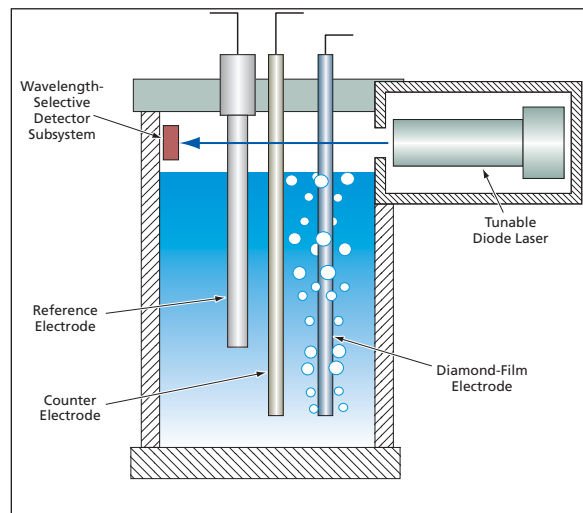
Inquiries concerning rights for the commercial use of this invention should be addressed to NASA Glenn Research Center, Innovative Partnerships Office, Attn: Steven Fedor, Mail Stop 4-8, 21000 Brookpark Road, Cleveland, Ohio 44135. Refer to LEW-18623-1.

Spectroelectrochemical Instrument Measures TOC

No hazardous reagents, ultraviolet light, or high temperature are needed.

Goddard Space Flight Center, Greenbelt, Maryland

A spectroelectrochemical instrument has been developed for measuring the total organic carbon (TOC) content of an aqueous solution. Measurements of TOC are frequently performed in environmental, clinical, and industrial settings. Until now, techniques for performing such measurements have included, variously, the use of hazardous reagents, ultraviolet light, or ovens, to promote reactions in which the carbon contents are oxidized. The instrument now being developed is intended to be a safer, more economical means of oxidizing organic carbon and determining the TOC levels of aqueous solutions and for providing a low power/mass unit for use in planetary missions.



CO₂ Would Be Produced by electrochemical oxidation of organic constituents of the aqueous solution, and the concentration of CO₂ in the headspace above the solution would be inferred from infrared absorption.

The proposed instrument exploits an electrochemical-oxidation principle that has also been investigated as the basis of a method of disposing of toxic organic industrial wastes. The method has found limited use, largely because the most common electrode materials (non-diamond carbon-based materials and such metals as platinum, silver, gold, mercury, and nickel) eventually become fouled or oxidized when operated at the high anodic potentials (between 2 and 2.5 V versus a standard hydrogen electrode) needed for efficient oxidation of organic compounds. An effort to overcome this limitation has led to consideration of electrodes consisting of substrate materials (e.g. silicon or tita-

nium) coated with diamond that has been heavily doped with boron to promote p-type semiconductivity to a nearly metallic level. Such boron-doped diamond (BDD) electrodes have been found to be robust, capable of withstanding high anodic potentials, and resistant to self-oxidation.

This new TOC instrument (see figure) includes a BDD electrode, a counter

electrode, and a reference electrode in a cell containing an aqueous solution to be tested. A positive potential of about 2.5 V versus the reference electrode is applied to the BDD electrode to cause the organic material in the solution to become oxidized, thereby producing H₂O and CO₂. A headspace above the solution traps escaping CO₂. The concentration of the CO₂ can be measured by a minia-

ture infrared absorption spectrometer comprised of a tunable diode laser and an associated wavelength-selective detector subsystem. The TOC of the solution is proportional to the concentration of CO₂ in the headspace.

This work was done by Sam Kounaves at Tufts University for Goddard Space Flight Center. Further information is contained in a TSP (see page 1). GSC-14814-1



A Miniaturized Video System for Monitoring *Drosophila* Behavior

This method allows monitoring the movement of many fruit flies in space simultaneously.

Ames Research Center, Moffett Field, California

Long-term spaceflight may induce a variety of harmful effects in astronauts, resulting in altered motor and cognitive behavior. The stresses experienced by humans in space — most significantly weightlessness (microgravity) and cosmic radiation — are difficult to accurately simulate on Earth. In fact, prolonged and concomitant exposure to microgravity and cosmic radiation can only be studied in space.

Behavioral studies in space have focused on model organisms, including *Drosophila melanogaster*. *Drosophila* is often used due to its short life span and generational cycle, small size, and ease of maintenance. Additionally, the well-characterized genetics of *Drosophila* behavior on Earth can be applied to the analysis of results from spaceflights, provided that the behavior in space is accurately recorded.

In 2001, the BioExplorer project introduced a low-cost option for researchers: the small satellite. While this approach enabled multiple inexpensive launches of biological experiments, it also imposed stringent restrictions on the monitoring systems in terms of size, mass, data bandwidth, and power consumption. Suggested parameters for size are on the order of 100 mm³ and 1 kg mass for the entire payload. For *Drosophila* behavioral studies, these engineering requirements are not met by commercially available systems.

One system that does meet many requirements for behavioral studies in space is the actimeter. Actimeters use infrared light gates to track the number of

times a fly crosses a boundary within a small container (3×3×40 mm). Unfortunately, the apparatus needed to monitor several flies at once would be larger than the capacity of the small satellite.

A system is presented, which expands on the actimeter approach to achieve a highly compact, low-power, ultra-low bandwidth solution for simultaneous monitoring of the behavior of multiple flies in space. This also provides a simple, inexpensive alternative to the current systems for monitoring *Drosophila* populations in terrestrial experiments, and could be especially useful in field experiments in remote locations. Two practical limitations of the system should be noted: first, only walking flies can be observed — not flying — and second, although it enables population studies, tracking individual flies within the population is not currently possible.

The system used video recording and an analog circuit to extract the average light changes as a function of time. Flies were held in a 5-cm diameter Petri dish and illuminated from below by a uniform light source. A miniature, monochrome CMOS (complementary metal-oxide semiconductor) video camera imaged the flies. This camera had automatic gain control, and this did not affect system performance. The camera was positioned 5–7 cm above the Petri dish such that the imaging area was 2.25 cm². With this basic setup, still images and continuous video of 15 flies at one time were obtained. To reduce the required data bandwidth by several orders of magnitude, a band-pass filter (0.3–10

Hz) circuit compressed the video signal and extracted changes in image luminance over time. The raw activity signal output of this circuit was recorded on a computer and digitally processed to extract the fly movement “events” from the waveform. These events corresponded to flies entering and leaving the image and were used for extracting activity parameters such as inter-event duration. The efficacy of the system in quantifying locomotor activity was evaluated by varying environmental temperature, then measuring the activity level of the flies.

The system presented in this work for monitoring fly activity is an inexpensive, compact, and ultra-low bandwidth alternative to currently available options, making it a suitable candidate for biological experiments on small satellites or field experiments. In contrast to most actimeters, multiple flies can be imaged in a small apparatus. Additionally, the flies are contained in a larger chamber (20 cm² vs., e.g., 1.2 cm²), which permits motion in two axes rather than one. This may allow the fly behavior to more closely approximate the natural state.

This work was done by Sharmila Bhattacharya of Ames Research Center; Omer Inan, Gregory Kovacs, and Mozziyar Etemadi of Stanford University; Max Sanchez of Lockheed Martin; and Oana Marcu of National Space Grant Foundation. Further information is contained in a TSP (see page 1).

Inquiries concerning rights for commercial use of this invention should be addressed to the Ames Technology Partnerships Division at (650) 604-5761. Refer to ARC-16338-1.

Hydrofocusing Bioreactor Produces Anti-Cancer Alkaloids

Enhancement of production may be attributable to favorable aggregation of cells.

Lyndon B. Johnson Space Center, Houston, Texas

A methodology for growing three-dimensional plant tissue models in a hydrodynamic focusing bioreactor (HFB) has been developed. The methodology is expected to be widely applicable,

both on Earth and in outer space, as a means of growing plant cells and aggregates thereof under controlled conditions for diverse purposes, including research on effects of gravitation and

other environmental factors upon plant growth and utilization of plant tissue cultures to produce drugs in quantities greater and at costs lower than those of conventional methodologies.

The HFB was described in "Hydrofocusing Bioreactor for Three-Dimensional Cell Culture" (MSC-22358), *NASA Tech Briefs*, Vol. 27, No. 3 (March 2003), page 66. To recapitulate: The HFB offers a unique hydrofocusing capability that enables the creation of a low-shear liquid culture environment simultaneously with the "herding" of suspended cells and tissue assemblies and removal of unwanted air bubbles. The HFB includes a rotating cell-culture vessel with a centrally located sampling port and an internal rotating viscous spinner attached to a rotating base. The vessel and viscous spinner can be made to rotate at the same speed and direction or different speeds and directions to tailor the flow field and the associated hydrodynamic forces in the vessel in order to obtain low-shear suspension of cells and control of the locations of cells and air bubbles.

For research and pharmaceutical-production applications, the HFB offers two major benefits: low shear stress, which promotes the assembly of cells into tissue-like three-dimensional constructs;

and randomization of gravitational vectors relative to cells, which affects production of medicinal compounds. Presumably, apposition of plant cells in the absence of shear forces promotes cell-cell contacts, cell aggregation, and cell differentiation. Only gentle mixing is necessary for distributing nutrients and oxygen.

It has been postulated that inasmuch as cells in the simulated microgravitation of an HFB do not need to maintain the same surface forces as in normal Earth gravitation, they can divert more energy sources to growth and differentiation and, perhaps, to biosynthesis of greater quantities of desired medicinal compounds. Because one can adjust the HFB to vary effective gravitation, one can also test the effects of intermediate levels of gravitation on biosynthesis of various products.

The potential utility of this methodology for producing drugs was demonstrated in experiments in which sandalwood and Madagascar periwinkle cells were grown in an HFB. The conditions

in the HFB were chosen to induce the cells to form into aggregate cultures that produced anti-cancer indole alkaloids in amounts greater than do comparable numbers of cells of the same species cultured according to previously known methodologies. The observations made in these experiments were interpreted as suggesting that the aggregation of the cells might be responsible for the enhancement of production of alkaloids.

This work was done by Steve R. Gonda of Johnson Space Center and Jagan V. Valluri of Marshall University. Further information is contained in a TSP (see page 1).

In accordance with Public Law 96-517, the contractor has elected to retain title to this invention. Inquiries concerning rights for its commercial use should be addressed to:

Dr. Jagan V. Valluri

Marshall University

6242 Highland Dr.

Huntington, WV 25705

E-mail: valluri@marshall.edu

Refer to MSC-24199-1, volume and number of this NASA Tech Briefs issue, and the page number.



Creep Measurement Video Extensometer

This automated system measures test-sample creep rates for materials testing.

John H. Glenn Research Center, Cleveland, Ohio

Understanding material behavior under load is critical to the efficient and accurate design of advanced aircraft and spacecraft. Technologies such as the one disclosed here allow accurate creep measurements to be taken automatically, reducing error.

Before the present innovation, there was no satisfactory method of accurately measuring the mechanical strain characteristics of materials during deformation at high temperatures inside an inert gas or vacuum chamber. The goal was to develop a non-contact, automated system capable of capturing images that could subsequently be processed to obtain the strain characteristics of these materials during deformation, while maintaining adequate resolution to capture the true deformation response of the material.

The measurement system comprises a high-resolution digital camera, computer, and software that work collectively to interpret the image. The camera captures an image of the specimen prior to beginning the test. The image, containing two fiducial marks at a known distance, is analyzed by the software to determine the relationship between actual

distance and the number of pixels separating the fiducials in the image. This is the basic calibration prior to the beginning of a test.

Once a test is started, images are captured at a predetermined rate and the calibration relationship is used to determine the distance between the fiducials while the specimen is being deformed, by converting the pixel distance between fiducials to the actual separation distance via the predetermined relationship. The separation distance is then used to measure the creep rate, and information important to the analysis of the test is automatically written to a file that can be exported to other analytical software. This system can also be used for tensile and compression testing, but data acquisition rates are limited due to the current state-of-the-art in hardware. Finally, the system has been proven out for testing being conducted at low temperature, high temperature, in air, vacuum, and inert gas environments, on systems that give line-of-sight access either directly or via a chamber viewport.

The software for this technology was written in LabVIEW, C, and VBScript. LabVIEW was used for the majority of

the code (user interface, program control, data storage, etc.). Standard image processing algorithms were written in C for those areas of the code requiring computationally intensive image processing routines (connected components labeling, circular Hough transform, and circularity measurement). VBScript is used to control the cameras and transfer images from the cameras to the PC. The VBScript uses Windows Imaging Acquisition (WIA) to send commands to the cameras and is based on sample code from Microsoft and a script called "Camera Control."

The system, based on an inexpensive, 12-megapixel, digital SLR camera, provides an accuracy that is within 0.0005 in. (12.8 μm). In contrast, the prior art (optical cathetometry) was only accurate to within 0.001 in. (25.4 μm). Hence, increased accuracy was not only achieved, but can be further increased by using even higher-resolution cameras (when available) or increased magnifications where applications permit.

This work was done by Mark Jaster, Mary Vickerman, Santo Padula II, and John Juhas of Glenn Research Center. Further information is contained in a TSP (see page 1). LEW-18578-1

Radius of Curvature Measurement of Large Optics Using Interferometry and Laser Tracker

This method determines the curvature radius of large mirrors.

Goddard Space Flight Center, Greenbelt, Maryland

The determination of radius of curvature (ROC) of optics typically uses either a phase measuring interferometer on an adjustable stage to determine the position of the ROC and the optics surface under test. Alternatively, a spherometer or a profilometer are used for this measurement.

The difficulty of this approach is that for large optics, translation of the interferometer or optic under test is problematic because of the distance of translation

required and the mass of the optic. Profilometry and spherometry are alternative techniques that can work, but require a profilometer or a measurement of sub-apertures of the optic. The proposed approach allows a measurement of the optic figure simultaneous with the full aperture radius of curvature.

The steps required for this measurement are:

- Alignment of the phase measuring interferometer with the optic under test.

For a spherical optic, a transmission sphere that overfills (faster f#) the optic is used.

- The power is nulled by translating the optic under test (OUT) or the interferometer. At this point, the transmission sphere focus is the radius of curvature of the OUT.
- An adjustable mount near the focus of the transmission sphere has a magnetic nest for placing a laser tracker retro-target. This is a spherical target

with a cube corner inset co-aligned with the center of the sphere. These devices are available commercially.

- The laser tracker target is then placed in the calibration nest of the laser tracker, zeroed, and hand-carried to the position of the laser tracker nest near the interferometer. The laser tracker beam must be continuously locked to the tracker to stay in lock. This is a typical mode of the laser tracker used for absolute metrology.
- The spherical laser tracker is positioned so that the shiny (non-retro)

surface of the tracker target is aligned to the transmission sphere. It is then translated until a nulled interferogram is observed. At this point, the center of the laser tracker target is at the focus of the transmission sphere (and thereby at the ROC of the OUT.)

- The x,y,z position of the tracker target is then acquired by the laser tracker.
- The laser tracker target is then removed from the nest, and without losing lock to the tracker, is hand-carried to the OUT. It is then placed on the OUT at its center (which has a nest on its surface pre-aligned to the center).

- The tracker then acquires the x,y,z position of the laser tracker target.
- The data is reduced and the two positions calculated. The position at the ROC is directly at the ROC, while the position on the mirror is displaced by the radius of the laser tracker target. This radius must be added to the distance measurement in the calculation.

This process is repeated to allow redundancy of the measurement.

This work was done by John Hagopian and Joseph Connelly of Goddard Space Flight Center. Further information is contained in a TSP (see page 1). GSC-15941-1

n-B-pi-p Superlattice Infrared Detector

NASA's Jet Propulsion Laboratory, Pasadena, California

A specially designed barrier (B) is inserted at the n-pi junction [where most G-R (generation-recombination) processes take place] in the standard n-pi-p structure to substantially reduce generation-recombination dark currents. The resulting n-B-pi-p structure also has reduced tunneling dark currents, thereby solving some of the limitations to which current type II strained layer superlattice infrared detectors are prone. This innovation is compati-

ble with common read-out integrated circuits (ROICs).

This work was done by David Z. Ting, Sumith V. Bandara, Cory J. Hill, and Sarath D. Gunapala of Caltech for NASA's Jet Propulsion Laboratory. For more information, contact iaoffice@jpl.nasa.gov.

In accordance with Public Law 96-517, the contractor has elected to retain title to this invention. Inquiries concerning rights for its commercial use should be addressed to:

*Innovative Technology Assets Management
JPL*

Mail Stop 202-233

4800 Oak Grove Drive

Pasadena, CA 91109-8099

E-mail: iaoffice@jpl.nasa.gov

Refer to NPO-46171, volume and number of this NASA Tech Briefs issue, and the page number.



Safe Onboard Guidance and Control Under Probabilistic Uncertainty

NASA's Jet Propulsion Laboratory, Pasadena, California

An algorithm was developed that determines the fuel-optimal spacecraft guidance trajectory that takes into account uncertainty, in order to guarantee that mission safety constraints are satisfied with the required probability. The algorithm uses convex optimization to solve for the optimal trajectory. Convex optimization is amenable to onboard so-

lution due to its excellent convergence properties.

The algorithm is novel because, unlike prior approaches, it does not require time-consuming evaluation of multivariate probability densities. Instead, it uses a new mathematical bounding approach to ensure that probability constraints are satisfied, and it is shown that the result-

ing optimization is convex. Empirical results show that the approach is many orders of magnitude less conservative than existing set conversion techniques, for a small penalty in computation time.

This work was done by Lars James Blackmore of Caltech for NASA's Jet Propulsion Laboratory. For more information, contact iaoffice@jpl.nasa.gov. NPO-46155

General Tool for Evaluating High-Contrast Coronagraphic Telescope Performance Error Budgets

NASA's Jet Propulsion Laboratory, Pasadena, California

The Coronagraph Performance Error Budget (CPEB) tool automates many of the key steps required to evaluate the scattered starlight contrast in the dark hole of a space-based coronagraph. The tool uses a Code V prescription of the optical train, and uses MATLAB programs to call ray-trace code that generates linear beam-walk and aberration sensitivity matrices for motions of the optical elements and line-of-sight pointing, with and without controlled fine-steering mirrors (FSMs). The sensitivity matrices are imported by macros into Excel 2007, where the error budget is evaluated. The user specifies the particular optics of interest, and chooses the quality of each optic from a predefined set of PSDs. The spreadsheet creates a nominal set of thermal and jitter motions, and combines that with the sensitivity matrices to generate an error budget for the system.

CPEB also contains a combination of form and ActiveX controls with Visual Basic for Applications code to allow for user interaction in which the user can perform trade studies such as changing engineering requirements, and identifying and isolating stringent requirements. It contains summary tables and graphics that can be instantly used for reporting results in view graphs.

The entire process to obtain a coronagraphic telescope performance error budget has been automated into three stages: conversion of optical prescription from Zemax or Code V to MACOS (in-house optical modeling and analysis tool), a linear models process, and an error budget tool process. The first process was improved by developing a MATLAB package based on the Class Constructor Method with a number of user-defined functions that allow the user to modify the MACOS optical pre-

scription. The second process was modified by creating a MATLAB package that contains user-defined functions that automate the process. The user interfaces with the process by utilizing an initialization file where the user defines the parameters of the linear model computations. Other than this, the process is fully automated. The third process was developed based on the Terrestrial Planet Finder coronagraph Error Budget Tool, but was fully automated by using VBA code, form, and ActiveX controls.

This work was done by Luis F. Marchen of Caltech for NASA's Jet Propulsion Laboratory. For more information, contact iaoffice@jpl.nasa.gov.

This software is available for commercial licensing. Please contact Daniel Broderick of the California Institute of Technology at danielb@caltech.edu. Refer to NPO-47220.

Hidden Statistics of Schrödinger Equation

NASA's Jet Propulsion Laboratory, Pasadena, California

Work was carried out in determination of the mathematical origin of randomness in quantum mechanics and creating a hidden statistics of Schrödinger equation; i.e., to expose the transitional sto-

chastic process as a "bridge" to the quantum world. The governing equations of hidden statistics would preserve such properties of quantum physics as superposition, entanglement, and direct-pro-

duct decomposability while allowing one to measure its state variables using classical methods. In other words, such a system would reinforce the advantages and minimize the limitations of both quan-

tum and classical aspects, and therefore, it will be useful for implementation of quantum computing.

Recent advances in quantum information theory have inspired an explosion of interest in new quantum algorithms for solving hard computational problems. Three basic “non-classical” properties of quantum mechanics — superposition, entanglement, and direct tensor-product decomposability — were main reasons for optimism about capabilities of quantum computers and

quantum communications as well as for a new approach to cryptography. However, one major problem is keeping the components of a quantum computer in a coherent state, as the slightest interaction with the external world would cause the system to decohere. Another problem is measurement: by the laws of quantum mechanics, a measurement yields a random and incomplete answer, and it destroys the stored state.

This proposed reinterpretation of quantum formalism opens up new ad-

vantages of quantum computers: if the Madelung equations are implemented on a classical scale (using, for instance, electrical circuits or optical devices), all the quantum effects important for computations would be preserved; at the same time, the problems associated with decoherence and measurement would be removed.

This work was done by Michail Zak of Caltech for NASA’s Jet Propulsion Laboratory. For more information, contact iaoffice@jpl.nasa.gov. NPO-46731

➤ Optimal Padding for the Two-Dimensional Fast Fourier Transform

Appending data to an optimum length decreases computing runtime.

Goddard Space Flight Center, Greenbelt, Maryland

One-dimensional Fast Fourier Transform (FFT) operations work fastest on grids whose size is divisible by a power of two. Because of this, padding grids (that are not already sized to a power of two) so that their size is the next highest power of two can speed up operations. While this works well for one-dimensional grids, it does not work well for two-dimensional grids.

For a two-dimensional grid, there are certain pad sizes that work better than others. Therefore, the need exists to generalize a strategy for determining optimal pad sizes. There are three steps in the FFT algorithm. The first is to perform a one-dimensional transform on each row in the grid. The second step is to transpose the resulting matrix. The third step is to perform a one-dimensional transform on each row in the resulting grid. Steps one and three both

benefit from padding the row to the next highest power of two, but the second step needs a novel approach.

An algorithm was developed that struck a balance between optimizing the grid pad size with prime factors that are small (which are optimal for one-dimensional operations), and with prime factors that are large (which are optimal for two-dimensional operations). This algorithm optimizes based on average run times, and is not fine-tuned for any specific application. It increases the amount of times that processor-requested data is found in the set-associative processor cache. Cache retrievals are 4–10 times faster than conventional memory retrievals.

The tested implementation of the algorithm resulted in faster execution times on all platforms tested, but with varying sized grids. This is because various computer architectures process commands

differently. The test grid was 512×512. Using a 540×540 grid on a Pentium V processor, the code ran 30 percent faster. On a PowerPC, a 256×256 grid worked best. A Core2Duo computer preferred either a 1040×1040 (15 percent faster) or a 1008×1008 (30 percent faster) grid.

There are many industries that can benefit from this algorithm, including optics, image-processing, signal-processing, and engineering applications.

This work was done by Bruce H. Dean, David L. Aronstein, and Jeffery S. Smith of Goddard Space Flight Center. Further information is contained in a TSP (see page 1).

This invention is owned by NASA, and a patent application has been filed. Inquiries concerning nonexclusive or exclusive license for its commercial development should be addressed to the Patent Counsel, Goddard Space Flight Center, (301) 286-7351. Refer to GSC-15678-1.

➤ Spatial Query for Planetary Data

This technology is extensible to Earth science and satellite monitoring and surveillance.

NASA’s Jet Propulsion Laboratory, Pasadena, California

Science investigators need to quickly and effectively assess past observations of specific locations on a planetary surface. This innovation involves a location-based search technology that was adapted and applied to planetary science data to support a spatial query capability for mission operations software.

Conventional databases of planetary datasets are indexed and searchable by various metadata, such as acquisition time,

phase of mission, and target. Searching these datasets will produce enormous datasets that are difficult, or impractical, to browse through to identify observations of very specific targets. For queries at specific locations, it is fundamentally more efficient to specify the location as the target of the query; and to have the database search based on the location of the data rather than metadata that is only indirectly or tangentially related to location.

High-performance location-based searching requires the use of spatial data structures for database organization. Spatial data structures are designed to organize datasets based on their coordinates in a way that is optimized for location-based retrieval. The particular spatial data structure that was adapted for planetary data search is the R+ tree. The R+ tree arranges data as a set of nodes that represents bounding rectangles. Every leaf

node in the tree is a particular datum with coordinates. The root node represents a bounding box containing the entire set of data. Each level of the tree subdivides the search space into smaller and smaller bounding rectangles, each containing a smaller subset of the data. A query on the R+ tree for a set of coordinates will follow one unique path from the root to the leaf, and return the data contained in the coordinates. The complexity of the search is bounded by the depth of the tree, so the R+ tree insertion

algorithm maintains a balanced tree such that the depth is minimized.

A map view provides an intuitive way to specify a set of coordinates for a location-based query. The software will let the user select any location on the map of the rover's traverse path to date and return all of the results in under a second. This was particularly useful during tactical activity planning when the question of "what data do we have of this location" is asked every day. The wrong answer to this question is very expensive: false neg-

atives result in missed science opportunities that may never come again, while false positives results in a waste of spacecraft time and bandwidth resources.

This work was done by Khawaja S. Shams, Thomas M. Crockett, Mark W. Powell, Joseph C. Joswig, and Jason M. Fox of Caltech for NASA's Jet Propulsion Laboratory.

The software used in this innovation is available for commercial licensing. Please contact Daniel Broderick of the California Institute of Technology at danielb@caltech.edu. Refer to NPO-46637.

➤ Higher Order Mode Coupling in Feed Waveguide of a Planar Slot Array Antenna

NASA's Jet Propulsion Laboratory, Pasadena, California

A simple technique was developed to account for the higher order mode coupling between adjacent coupling slots in the feed waveguide of a planar slot array. The method uses an equation relating the slot impedance to the slot voltage and a reaction integral involving the equivalent magnetic current of the slot aperture and the magnetic field coupled from an adjacent slot.

Most waveguide-fed slot antennas use centered-inclined coupling slots in the feed waveguides. In the proposed method, one uses the Elliott's design technique to determine tilt angles and

lengths of the coupling slots. The radiating slots are modeled as shunt admittances, and the coupling slots are modeled as series impedances.

By using reaction integrals to account for higher order mode coupling between adjacent coupling slots, the "active impedance" of each coupling slot is obtained, which differs from the original impedance by a small amount due to higher order mode coupling. The tilt angle and length of each coupling slot are perturbed so that the active impedance of each slot is the same as the corresponding starting value of the impedance before the iterative

process started. This process converges after three or four iterations and uses algebraic equations and fast reaction integrals.

Because of desirable features of waveguide arrays such as low volume, ease of design and manufacture, and ease of deployment, these antennas find applications in aeronautical and space activities. In addition, these all-metal antennas can withstand high radiation environments encountered in space.

This work was done by Sembiam Rengarajan of Caltech for NASA's Jet Propulsion Laboratory. For more information, contact iaoffice@jpl.nasa.gov. NPO-47419

➤ Evolutionary Computational Methods for Identifying Emergent Behavior in Autonomous Systems

NASA's Jet Propulsion Laboratory, Pasadena, California

A technique based on Evolutionary Computational Methods (ECMs) was developed that allows for the automated optimization of complex computationally modeled systems, such as autonomous systems. The primary technology, which enables the ECM to find optimal solutions in complex search spaces, derives from evolutionary algorithms such as the genetic algorithm and differential evolution. These methods are based on biological processes, particularly genetics, and define an iterative process that evolves parameter sets into an optimum.

Evolutionary computation is a method that operates on a population of existing computational-based engineering mod-

els (or simulators) and competes them using biologically inspired genetic operators on large parallel cluster computers. The result is the ability to automatically find design optimizations and trades, and thereby greatly amplify the role of the system engineer.

The ECM technique is extremely effective at quickly finding not only individual best solutions, but also an entire collection of best solutions for all possible ranges of conditions. ECM provides an efficient standard of performance that specifies the best solution given a set of requirements or goals for all possible environmental variables. The ECM derived standard of performance can be

directly compared to actual performance to provide a test standard of reference. Comparison of the ECM best solutions with actual performance will identify where the deviations from optimum occurred leading to localization of problem areas. This includes illuminating deficiencies in simulation capabilities. Examination of the full set of ECM derived best performance will enable the identification and characterization of unexpected or emergent behaviors.

This work was done by Richard J. Terrill and Alexandre Guillaume of Caltech for NASA's Jet Propulsion Laboratory. For more information, contact iaoffice@jpl.nasa.gov. NPO-46686

▶ Sampling Theorem in Terms of the Bandwidth and Sampling Interval

Goddard Space Flight Center, Greenbelt, Maryland

An approach has been developed for interpolating non-uniformly sampled data, with applications in signal and image reconstruction. This innovation generalizes the Whittaker-Shannon sampling theorem by emphasizing two assumptions explicitly (definition of a band-limited function and construction by periodic extension). The Whittaker-Shannon sampling theorem is thus expressed in terms of two funda-

mental length scales that are derived from these assumptions. The result is more general than what is usually reported, and contains the Whittaker-Shannon form as a special case corresponding to Nyquist-sampled data. The approach also shows that the preferred basis set for interpolation is found by varying the frequency component of the basis functions in an optimal way.

This work was done by Bruce H. Dean of Goddard Space Flight Center. For further information, contact the Goddard Innovative Partnerships Office at (301) 286-5810.

This invention is owned by NASA, and a patent application has been filed. Inquiries concerning nonexclusive or exclusive license for its commercial development should be addressed to the Patent Counsel, Goddard Space Flight Center, (301) 286-7351. Refer to GSC-15685-1.



Meteoroid/Orbital Debris Shield Engineering Development Practice and Procedure

A document describes a series of models created for the determination of the probability of survival of critical spacecraft components from particle strike damage caused by hypervelocity impact of meteoroids and/or orbital debris. These models were integrated with both shield design and hypervelocity impact testing to develop adequate protection of said components to meet mission survivability requirements.

Spacecraft configuration and construction were determined, including geometric shapes, dimensions, positions, material of construction, etc., for the spacecraft or component. The types and levels of damage allowable for each protected component were determined.

Critical damage was defined by the damage level that will cause loss of function of the protected component. Required probability of survival for the critical components was determined. This was done by determining the probability of survival based on exposure only, neglecting shielding. Next, a Monte Carlo simulation was run representing all possible particle impacts, collecting data on shielding-protecting components. An empirical physics-based model that estimates the incident kinetic energy required to cause critical damage to the component was applied to each Monte Carlo simulated particle strike.

This work was done by James G. Zwitter and Marc A. Adams of Caltech for NASA's Jet Propulsion Laboratory. NPO-46082

Self-Balancing, Optical-Center-Pivot, Fast-Steering Mirror

A complete, self-contained fast-steering-mirror (FSM) mechanism is reported consisting of a housing, a mirror and mirror-mounting cell, three PZT (piezoelectric) actuators, and a counterbalance mass. Basically, it is a comparatively stiff, two-axis (tip-tilt), self-balanced FSM. Prior technology required two systems

back-to-back on a center bulkhead, employing six opposing actuators, which must then be electronically balanced and recalibrated from time to time. The present invention requires only three (or three pairs for flight redundancy) actuators. If a PZT actuator degrades, the inherent balance remains, and compensation for degraded stroke is made by simply increasing the voltage to the PZT. Prior designs typically do not pivot at the mirror optical center, creating unacceptable beam shear.

This work was done by James D. Moore and Johnathan W. Carson of Caltech for NASA's Jet Propulsion Laboratory. NPO-45985

Wireless Orbiter Hang-Angle Inclinometer System

A document describes a system to reliably gather the hang-angle inclination of the orbiter. The system comprises a wireless handheld master station (which contains the main station software) and a wireless remote station (which contains the inclinometer sensors, the RF transceivers, and the remote station software). The remote station is designed to provide redundancy to the system. It includes two RF transceivers, two power-management boards, and four inclinometer sensors.

Power-management algorithms were developed and implemented to assure nominal system operation over the elapsed time between when the inclinometer system is installed at the orbiter processing facility (OPF), and the actual hang-angle measurement operation when the orbiter is brought up to a full vertical position in the vehicle assembly building (VAB). Relay and polling schemes were implemented to overcome any RF interference and power-management schemes, respectively. A set of unique algorithms was also developed to take full advantage of the redundancy of the system to meet the critical measurement requirements.

Several novel features of the wireless hang-angle inclinometer system are an ultra-low thermal expansion coefficient mounting bracket, housing the inclinometer sensors, to minimize errors caused by thermal expansion over the

wide temperature range; a power management software to monitor and conserve electrical energy of the batteries in the remote station; and an RF health check algorithm to verify/assure proper communication link between the remote station and the hand-held base station.

This work was done by Angel Lucena, Jose Perotti, Eric Green, and Jonathan Byon of Kennedy Space Center; Bradley Burns, Carlos Mata, and John Randazzo of ASRC Aerospace Corporation; and Norman Blalock of Sierra Lobo, Inc. KSC-12751

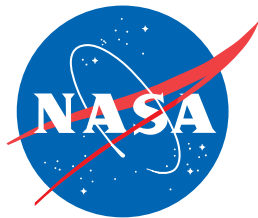
Internal Electrostatic Discharge Monitor — IESDM

A document discusses an innovation designed to effectively monitor dielectric charging in spacecraft components to measure the potential for discharge in order to prevent damage from internal electrostatic discharge (IESD). High-energy electrons penetrate the structural materials and shielding of a spacecraft and then stop inside dielectrics and keep accumulating. Those deposited charges generate an electric field. If the electric field becomes higher than the breakdown threshold ($\approx 2 \times 10^5$ V/cm), discharge occurs.

This monitor measures potentials as a function of dielectric depth. Differentiation of potential with respect to the depth yields electric field. Direct measurement of the depth profile of the potential in a dielectric makes real-time electronic field evaluation possible without simulations.

The IESDM has been designed to emulate a multi-layer circuit board, to insert very thin metallic layers between the dielectric layers. The conductors serve as diagnostic monitoring locations to measure the deposited electron-charge and the charge dynamics. Measurement of the time-dependent potential of the metal layers provides information on the amount of charge deposited in the dielectrics and the movement of that charge with time (dynamics).

This work was done by Wousik Kim, Dan M. Goebel, Insoo Jun, and Henry B. Garrett of Caltech for NASA's Jet Propulsion Laboratory. NPO-47347



National Aeronautics and
Space Administration